Data Fusion and Commercial Unmanned Aerial Vehicle Applications for First Responders

A thesis submitted by

Casey Corrado

In partial fulfillment of the requirements for the degree of

Master of Science

in

Mechanical Engineering

Tufts University

May 2017

Advisors: Dr. Karen Panetta, Dr. William Messner, Dr. Jason Rife

Abstract

Data Fusion and Commercial Unmanned Aerial Vehicle Applications for First Responders

by Casey Corrado

The commercial unmanned aerial vehicle (UAV) market is dominated by vehicles designed specifically for photography, with few UAVs possessing sensing capabilities beyond vision or thermal imaging. While relatively affordable and readily available, these UAVs have limited effectiveness in the field of emergency response. These existing UAVs, however, can be improved through sensor integration to make them applicable to emergency response. The focus of this thesis is to develop a UAV system designed for disasters involving radiation. This is done by combining radiation detection, imaging, and a global positioning system (GPS) with a commercial UAV to create a vehicle that can assess the affected region following a potentially radioactive incident. The challenges associated with using low cost commercial UAVs in disaster assessment, including data transmission range, endurance, payload, and control range, were also investigated.

Acknowledgements

I would like to thank Dr. Karen Panetta for being a wonderful mentor over the last three years - working in her lab has been a pleasure and joy. Thank you to Dr. William Messner, who served as my advisor for over five years and encouraged me every step of the way. I would also like to thank Dr. Jason Rife, who supported my research even before I had taken any of his classes.

Thank you to the other members of the First Responders project, Victor and Richard, who were invaluable teammates in this work. I wish them good luck as they continue working on this research. I would also like to thank all of the other amazing students in Professor Panetta's lab, as well as Warren in the Electrical Engineering Department.

Thank you to Jen, who made graduate school almost as much fun as it was stressful.

Lastly I would like to thank my parents – without them none of this would have been possible.

Table of Contents

List of Figures

List of Tables

List of Abbreviations

COTS	**C**ommercial **O**ff **T**he **S**helf
FEA	**F**inite **E**lement **A**nalysis
FEM	**F**inite **E**lement **M**odeling
GPS	**G**lobal **P**ositioning **S**ystem
M	**M**ach Number
Re	**Re**ynolds's Number
UAV	**U**nmanned **A**erial **V**ehicles

1. Introduction

UAVs have a long history of use for military applications. Unmanned vehicles have become critical tools in the military's arsenal, with UAVs dominating in the fields of surveillance, intelligence, and reconnaissance [1]. In recent years, these devices have been used as a means to conduct military warfare, with both the United States and foreign governments using UAVs to conduct air strikes on remote targets in places like the Middle East, with astounding accuracy [2]. These vehicles have proven to be extremely beneficial to national security, as well as incredibly dangerous, if misused. The abuse of these powerful systems could result in countless potential safety and security issues, even in non-military environments. Further complicating this issue is the growth of the commercial UAV market. There are many commercial off-the-self (COTS) UAVs available for the public to purchase. The use of UAVs for aerial photography has become increasingly popular, attracting both professional and amateur hobbyists [3]. Many companies have started to integrate the use of these devices for commercial purposes, such as the possibility of using UAVs to make same-day package deliveries [4]. With such easy access to these vehicles, there is an increased risk of them being used for terrorism or invasion of privacy.

While commercial UAVs pose a possible risk to security, they also show potential to improve health and safety. UAVs are now being used to monitor environmental conditions, such as pollution and air quality and the release of radiation from nuclear power plants [5]. Select local and state emergency response teams have begun to use surveillance UAVs to help with issues like search and rescue [6].

Several companies are even developing UAVs specifically designed for law enforcement [7]. One of the most promising applications for UAVs, however, is the field of emergency response and assessment. These vehicles can be used to map a disaster area, giving first responders important situational information following an incident such as a terrorist attack or natural disaster. This not only reduces the risk for first responders, but decreases the time it takes them to act on a scene and reach potential survivors.

A majority of UAVs used to assess disaster situations rely solely on vision capabilities. For example, following the Fukushima Nuclear Power Plant disaster, UAVs were used to take aerial photos of damaged reactors [8]. While these images were able to provide invaluable information about the damage, it would have been beneficial to have other sensor information. The addition of radiation detection, for example, could have been used to map radiation levels throughout the affected area. Another example is the use of UAVs as tools for wildfire assessment. With the addition of thermal imaging, responders are able to track wildfire growth [9]. With minimal sensing capabilities, however, existing UAVs have limited effectiveness when responding to dangerous situations.

Sensor integration and data fusion can be used to improve existing UAVs, allowing them to be used as more effective tools in the field of disaster response. UAVs can be customized for various situations through the integration of different sensors. The selection process for a specific sensor is dependent on the constraints of the system. For example, a lighter weight low resolution sensor might be chosen over a heavier high resolution sensor because of weight limitations. It is necessary to

2

reach a balance between the required sensitivity and resolution of a sensor and the limitations of the UAV, getting the best data possible without compromising other aspects of the system.

Once it is determined what sensors are best suited for a situation, data fusion can be used to create clear and useful information about the scene. In the case of radiation, for example, GPS data can be combined with radiation values to create a map of the radiation levels present in the affected area. Additional post processing elements can be used to further increase the information obtained from the UAV data. For example, image enhancement and facial recognition can be performed on aerial images obtained in flight [10]. Data fusion and sensor integration are the keys to improving existing commercial off-the-shelf UAVs for use in emergency response and assessment.

2. Design Scenario

As previously discussed, emergencies involving radiation are particularly challenging for human responders due to the increased health risks associated with radiation exposure. The time it takes first responders to act on the scene is prolonged due to the added safety measures, resulting in an increased response time to reach potential survivors. This makes disasters involving the release of radioactive material prime candidates for the use of unmanned vehicles; the technology can be used to assess and map an area before responders enter, increasing the efficiency of the response team, lowering safety risks for responders, and decreasing the overall response time. A commercially available surveillance UAV combined with radiation detection can be used to successfully complete this challenging task.

Teams responding to attacks involving dirty bombs could greatly benefit from the use of a radiation detecting UAV. Unlike a nuclear bomb, which can affect hundreds of square miles with large amounts of radiation, a dirty bomb often contains trace amounts of radiation and is mainly used to instill panic and slow down rescuer/investigator response times. [11]. The diffusion of radioactive particles after a dirty bomb explodes typically affects an area the size of a few city blocks [12]. This area sets the endurance and transmission requirements for the system. [1]

An investigation into existing commercial UAVs was conducted, with a price range

---

[1] It should be noted that the work presented focuses on smaller scale radioactive disasters, unlike the effects of nuclear bomb or a nuclear power plant failure.

of $300 to $13,000. It was determined that currently available units have a flight times of 10-30 minutes with a maximum speed between 10-25 m/s. This allows these UAVs to fly anywhere between 6-45 km. Adding additional sensing elements, however, affects the payload weight, drag, and power draw of the system, resulting in lower flight times and shorter maximum distances. Even before adding further sensing components, these UAVs are not capable of covering the entire affected area following a dirty bomb explosion. Environmental issues such as wind, rain, and physical topography pose additional challenges, making this task even more difficult. They can, however, be used as expendable tools to assess small affected regions following a disaster involving radioactive material, shortening the required flight time by eliminating the need to return.

In the event of a dirty bomb explosion, the majority of the radiation would be around the epicenter of the detonation. When responding to this, an inexpensive and expendable tool that evaluates the area, such as the proposed UAV system, would be incredibly useful. Data is transmitted back to responders in real time, allowing them to remotely assess the area. Sacrificing a relatively inexpensive and replaceable UAV is preferable to risking human life, especially if an armed assailant is still present in the area.

The creation of this UAV application presents a system integration problem. Additional sensing elements need to be added to a commercial UAV without significantly affecting flight time, making payload weight and power draw extremely important. To preserve flight time, the payload weight needs to be minimized and additional sensors can only use a small fraction of the UAV's

battery power. Beyond this, other issues include the range of both control and data transmission. The UAV must have a communication and data transmission range large enough that the operator can receive data and control flight from a safe distance. Other factors, like usability and cost, must also be taken into account. Most first responders will not become expert UAV pilots, so the device must be easy to operate without extensive training. Additionally, the device must be low cost so it is easy to replace following use.

3. Background

One of the key elements of the discussed system is the radiation detection component. To fully understand how the sensor evaluates radiation levels, several aspects of the detection process must be discussed. First, it is necessary to understand how radiation levels are measured and what levels have the potential to affect human health. Table 1 and Figure 1 below lists radiation sources and the average radiation dose a person absorbs, where colors are used to indicate the severity of the radiation levels [13]. These values are measured in Sieverts (Sv), the unit measurement for a dose of radiation[2] [14]. If absorbed all at once, 1 Sv will result in illness, while levels higher than 8 Sv will cause immediate death [13]. It should be noted that radiation exposure depends on both the field of radiation present and the time of exposure. Short term exposure in a highly radioactive field can have the same effect as long term exposure in a less radioactive field.

---

[2] Another common way of denoting radiation levels is using Roentgens (R), where 1 mR is equivalent to 0.01 mSv.

Table 1. Radiation dose a person absorbs for various radiation sources.

Incident	Radiation Amount
One arm X-Ray	1 uSv
Dental X-Ray	5 uSv
Chest X-Ray	20 uSv
Mammogram	3 mSv
Chest CT Scan	5.8 mSv
Maximum yearly dose permitted for US radiation workers	50 mSv
EPA yearly release limit for a nuclear power plant	250 mSv
Dose limit for emergency workers in lifesaving operations	250 mSv
Short Term Radiation Poisoning	400 mSv
Severe Radiation Poisoning	2000 mSv
Fatal Radiation Poisoning	8000 mSv
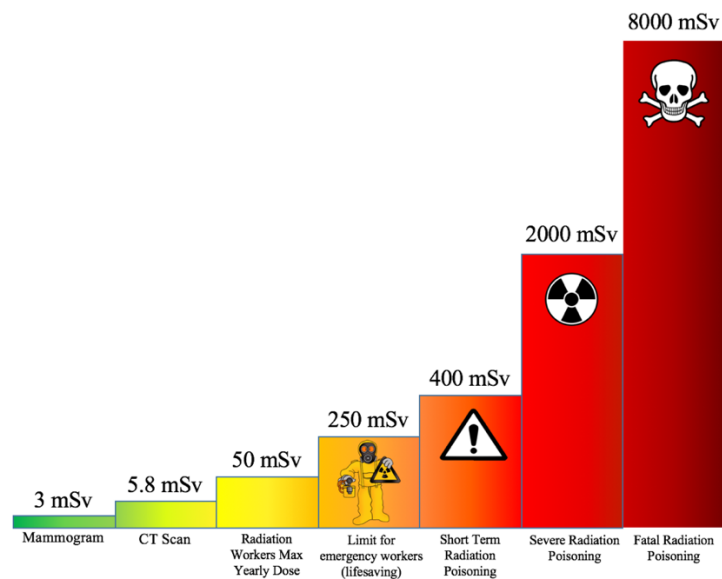
Fig. 1. Visual representation of various radiation levels.

Geiger counters and other radiation detecting devices use Geiger Muller Tubes to determine the radiation field in a space. This tube consists of an external cathode, a cylinder composed of an iron chromium alloy, and an internal anode that is surrounded by inert gases. The anode is biased at several hundred volts higher than the cathode, which creates a strong electric field. When either a gamma ray or a beta particle passes through the detection window, it causes an avalanche effect within the tube. The gas atoms become ionized and create more electron and positive ion pairs. The electric field causes these particles to accelerate the electrons towards the anode, ionizing even more gas molecules. This continues down the length of the tube, ionizing all the gas in a matter of microseconds. This ionization event creates a short current pulse, which is read as a voltage using an external resistor; this pulse corresponds to a count. After this event, the accumulated positive ions pair with electrons, counteracting the electric field. The tube is reverted back to its original state is ready for the next radiation event [15].
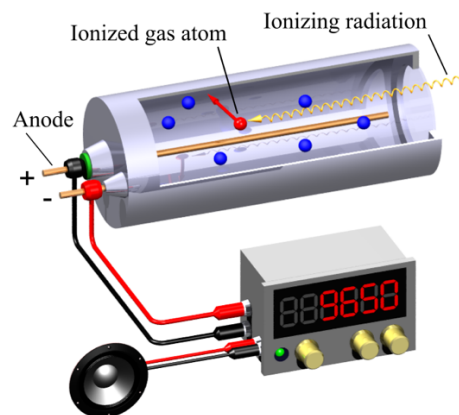
Fig. 2. Example Geiger Muller tube diagram [16].

As discussed above, Geiger Muller Tubes produce 'counts' when radiation is detected. Geiger counters and other radiation sensors then report radiation levels

9

using counts per minute (CPM). The higher the CPM in an area, the more radiation is present. Sensitivity is reported in the CPM the device can detect in a certain strength radiation field produced by a radioactive isotope, usually in Cesium-137 (137Cs) or Cobalt-60 (60Co) [17]. An example sensitivity rating for a Geiger Muller Tube might be 100 CPM in a radiative field of 0.01mSv/hour as produced by 137Cs. This means that a Geiger Counter using this tube would report 100 CPM in a field of 0.01mSv/hour, 200 CPM in a field of 0.02 mSv/hour for example. Additionally, a reading of 100 CPM would indicate that in one hour of exposure, a person would absorb about 0.01 mSv of radiation.

4. Prototype Development

Two different prototype designs were developed throughout the course of this research. The first proposed system, System A, utilized an existing commercial UAV system under development in Dr. Karen Panetta's Vision and Sensing Systems Laboratory. The work done for System A expands upon work done by previous researchers [10] and [17]. In [10], the authors developed a facial recognition system to be used with a commercial UAV. The authors in [17] then further developed the project and designed a radiation detection system suitable for use with UAVs. New work for this system focuses on the data fusion of this system with a commercial UAV, combining radiation detection with GPS position and live video capabilities to produce a UAV that can be used during disasters involving radioactive material.

After work was completed on System A, it was determined that the finished system would be unable to efficiently complete assessment tasks due to the outdated commercial UAV used, which was about four years old at the time of this research. Taking insight from completing System A, a new design, System B, was created using a newer commercial UAV model. Utilizing newer technology allowed for many additional features that would be impossible using the older model, such as automated flight. The creation of System B followed the same general guideline used for System A, where radiation detection was combined with GPS and live video capabilities of a commercial UAV. While System A was a fully functional, finalized prototype, System B serves as a proof of concept of using new UAV

technologies to accomplish the described task. System B lacks the fully completed

data transmission system and computer architecture contained in System A.

5. Proposed System A

As stated above, the first proposed system, System A, expands upon work done by previous researchers [10] and [17]. The task for finishing this system involved integrating the radiation sensor designed by [17] and completing the data fusion aspect.

5.1 System Components

This system is composed of two main components: the commercial UAV and the radiation sensor. In addition to describing these physical components, the following sections will also discuss the data fusion architecture of the design.

5.1.1 Commercial UAV

The researchers previously working on this project determined that the Draganfly X4-C, as seen in Figure 3, was a commercial UAV suitable for the design tasks. At the time of purchase, 2013, this UAV was one of the few affordable models with the features required for the project. At around $7,000, this UAV had a relatively long flight time and a suitable payload allowance. Additionally, the system had built-in GPS and vision capabilities, meaning that only the radiation detection component would need to be added.

Fig. 3. Commercial UAV used for System A, Draganfly X4-C.

This specific model used a XBee-PRO SE transmission system to transmit data from the UAV at a rate of 250 kbps. This system was used to continually transmit GPS coordinates, radiation levels, and other data back to the operator. Additionally, this UAV had live-video capabilities. The UAV transmits analog video from an attached GoPro Hero 3+, allowing for a continuous video feed. The camera is mounted on a 2-axis gimbal, both allowing for smooth video and operator control of camera angle and position. The UAV's video transmission system can be seen below in Figure 4.

Fig. 4. Video system used for System A Consists of a GoPro Hero 3 mounted on a 2-axis gimbal.

5.1.2 Radiation Detection

The weight and size of additional sensing components is incredibly important; the chosen sensors need to be light enough to meet the UAV's strict payload restrictions and small enough to not interfere with flight or camera movement. In addition, the radiation sensor must also be able to detect a large range of radiation levels. Both the amount of radiation and the exposure time are factors when determining the effects on human health, so the determined radiation readings can be used to determine the amount of time a responder can spend in a particular area. Given these restrictions, a radiation detection sensor developed by [17] was altered and added to the existing UAV system.

The radiation sensor developed in this design utilizes a T2417AC Geiger Muller Tube from Canberra Industries, which can be seen below in Figure 5. This device is capable of detecting both gamma and beta rays with a sensitivity of 450 CPM in a radiative field of 0.01 mSv/hour as produced by 137Cs. The device can detect levels as low as background radiation at 5 CPM, up to extremely high levels of 6.9 million CPM [17].

Fig. 5. Geiger Muller tube used in the System A radiation sensor.

The original circuit developed, seen on the left of Figure 6, was too large and bulky to be attached to the UAV. It was miniaturized into three connected pieces, two small circuit boards and the Geiger Muller tube, as seen on the right of Figure 6. This not only decreased the weight and overall size of the radiation sensor, but allowed for easier installation. It should be noted that the small Geiger Muller tube is used in both circuits, with protective tape wrapped around the tube in the newer model.
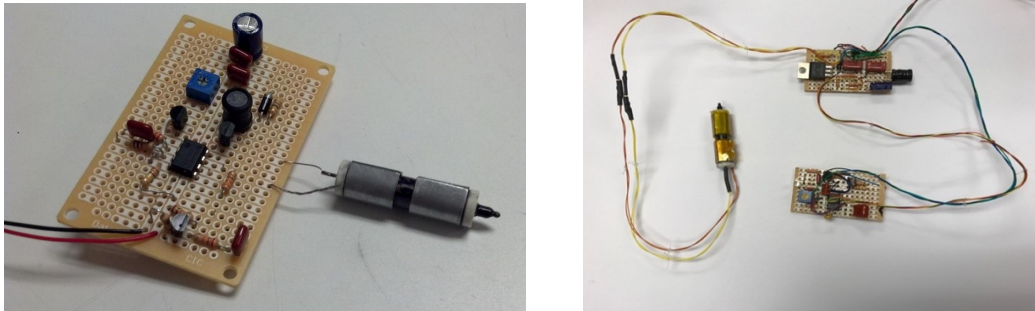
Fig. 6. Original (left) and altered (right) radiation sensors for System A.

5.1.3 Radiation Sensor Attachment

Once the radiation sensor was finalized, an attachment was designed to physically integrate the system with the UAV. Initially, the sensor was to be installed along the inside of the UAV's main cavity along with the other electronics, as shown in Figure 7. This would both protect the sensor from the elements, as well as keep the entire system balanced. It was determined, however, that installing the sensor that close to the other electrical components caused electromagnetic inference that affected data transmission.
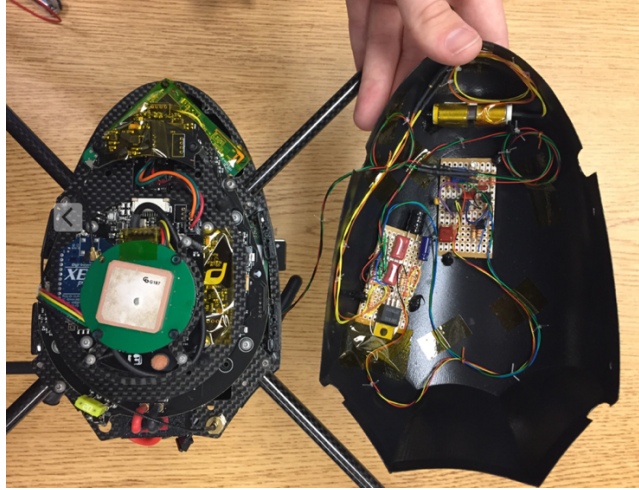
Fig. 7. Radiation sensor installed on the inside of the System A UAV main cavity.

After re-evaluating placement options, it was determined that the sensor could be attached to the camera's gimbal. This not only eliminated the problems associated with interference, but made the entire payload one single unit. This makes for easy removal or replacement in the event that the payload is damaged or needs to be switched out for a different system. Additionally, this keeps the payload weight directly under the UAV, keeping the entire system balanced. Any slight balance issues caused by the payload attachment can be compensated for by making small trim adjustments on the UAV's (X4-C's) controller.

To create the physical attachment, several design constraints were considered. The attachment needed to be lightweight in order to reduce payload weight, making material choice incredibly important. Additionally, the physical shape of the attachment needed to be carefully designed such that it only had minimal interference with the camera gimbal. Environmental conditions, such as wind or moisture, could damage the sensor's circuitry, so the attachment also needed to

provide environmental protection. Taking these constraints into consideration, an initial attachment prototype was created out of 3D printed plastic, PolyLactic Acid (PLA), as seen below in Figure 8.
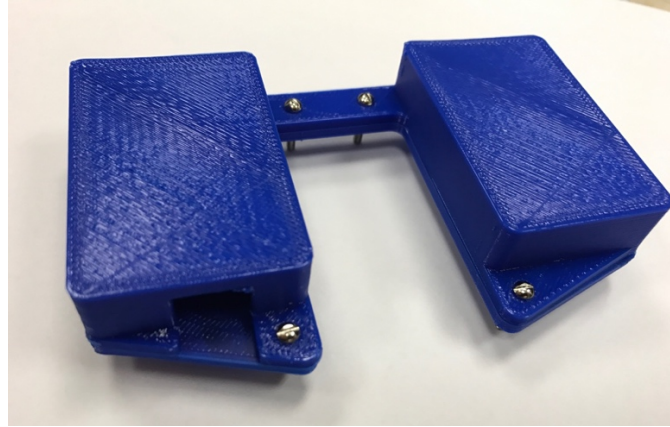
Fig. 8. Initial radiation sensor attachment prototype for System A.

The placement of the Geiger Muller tube posed a different set of challenges. This piece of the sensor needed to be attached to the UAV in a place that did not interfere with the detection of radioactive particles. As discussed earlier, this specific tube detects both gamma and beta radiation. Gamma radiation can be shielded by relatively thin layers of dense materials, such as lead, or by several feet of concrete [18]. Because the UAV and the attachment pieces are constructed out of plastic and carbon fiber, placement position will not interfere with detecting gamma radiation. The smaller beta particles, however, cause more of an issue. A thin layer of plastic is able to block beta particles, meaning that the Geiger Muller tube could not be installed inside the main cavity [18]. Additionally, the detection window of the tube needed to be unobstructed by the attachment; the detection window for this specific tube is the small area shown below in Figure 9.

Detection window

Fig. 9. Geiger Muller tube detection window for System A.

Taking these factors into consideration, it was determined that the tube attachment could be added to the radiation sensor attachment piece. As seen below in Figure 10, the Geiger Muller tube can be inserted into this attachment, leaving the detection window unobstructed.
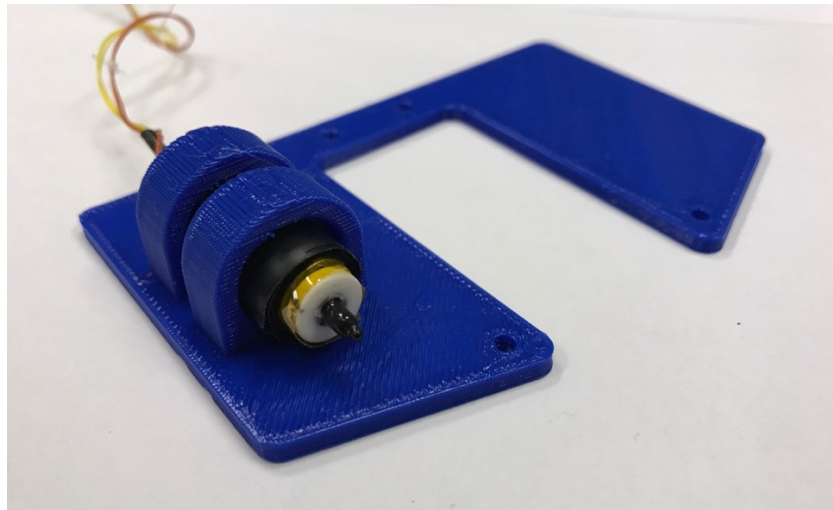
Fig. 10. Finalized Geiger Muller tube attachment for System A.

After several design iterations, the final attachment was 3D printed using carbon fiber and nylon, as seen in Figure 11. The combination of these two materials resulted in a strong and incredibly lightweight attachment piece. In addition, the nylon makes a seal around the carbon fiber, keeping the circuitry inside safe from environmental factors. The top piece connecting the Geiger Muller tube, however, was not able to be fabricated out of carbon fiber; the dimensions of the tube attachment were too small for nylon and carbon fiber layers to be printed together. Because of this, the top piece was printed using the PLA plastic used for the prototyping process. While slightly heavier than the intended carbon fiber, the small piece does not add significant weight to the payload and the plastic is strong enough to withstand the requirements of flight.
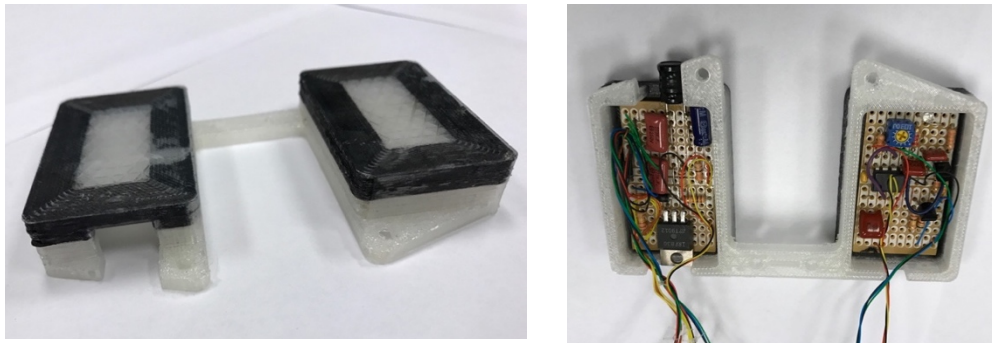
Fig. 11. Finalized carbon fiber attachment piece for radiation sensor in System A.

The completed radiation sensor attachment fits around the neck of the camera mount, and is connected via four screws; any exposed wires are taped down to the attachment. The completed payload can be seen below in Figure 12.
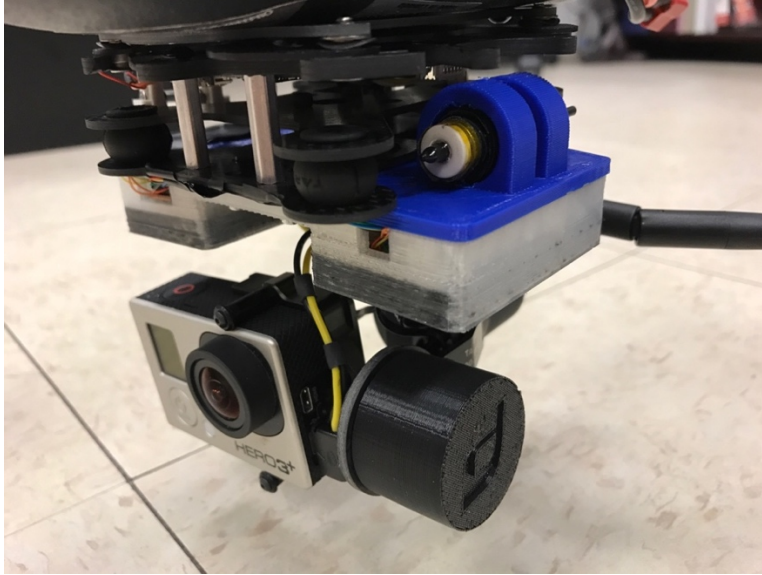
Fig. 12. Final assembled payload for System A.

It should be noted that the materials used were chosen specifically for event of a small dirty bomb explosion. The attachment piece would not, for example, be able to withstand the high temperatures associated with wildfires, which can exceed 800 °C. Both nylon and PLA had relatively low melting points, at about 260 °C and 180 °C respectively [19] [20]. It was assumed that the UAV would not be used in extremely high temperature situations, and different materials would be required for the attachment piece if this design constraint were to be included.

5.1.4 Data Fusion Architecture

The data fusion of radiation detection, GPS positioning, and live-video allow the discussed UAV to be used as a tool to quickly and efficiently map radiation levels in localized areas. The UAV flies over the affected zone and transmits GPS positioning and radiation data in real-time. A computer then interprets and maps

the radiation levels to determine what areas are unsafe. This data flow is represented in the block diagram below in Figure 13.
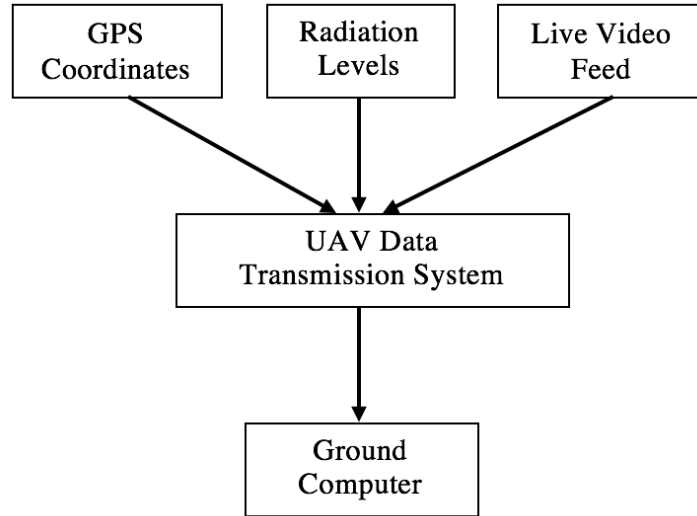
Fig. 13. Block diagram for the flow of data in System A.

The operator sees this information in the form of a GPS map, with colored radiation data overlaid. Green zones indicate areas that are safe to enter, while red indicates unsafe regions. This map utilizes open source MapQuest software to combine radiation and GPS data. In addition to the mapping element, the user interface also includes a live-video feed, as seen in Figure 14. This allows the operator to perform a visual assessment of the conditions in the area as well before entering the scene. For example, the camera can be used in conjunction with GPS data to find the location of potential survivors.
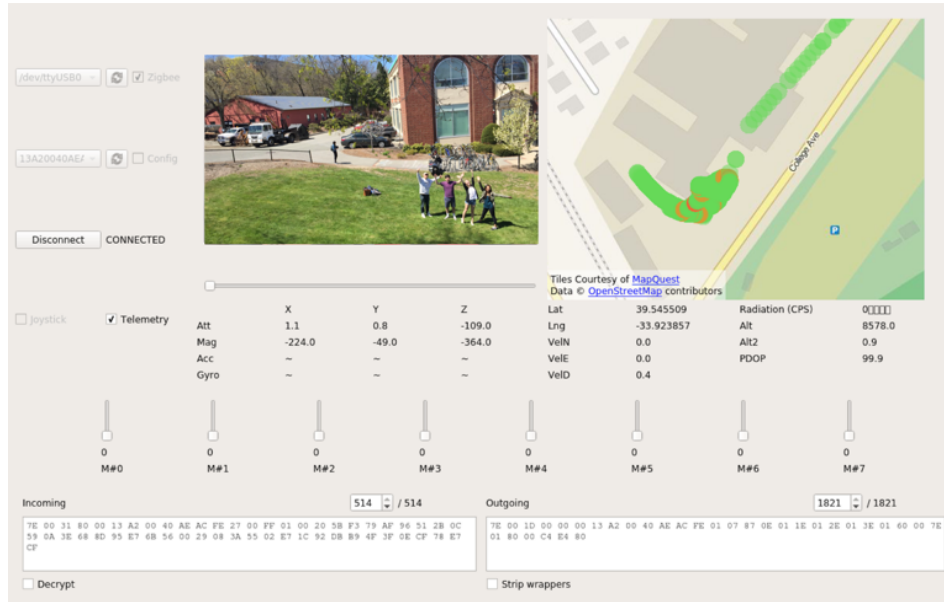
Fig. 14. User interface for System A. The connection controls are at the top left of the screen, where the operator can connect the computer to the UAV before flight. To the right is the live video feed, next to the GPS radiation map. Beneath these elements is the telemetry data, that gives information on variables like GPS location, radiation level (in counts per second), altitude, velocity, and others. Under this data is the incoming and outgoing data information. It can be used to determine the rate at which the computer is sending and receiving information.

One issue with the user interface discussed above was that the mapping element was dependent on external software. Mapquest was originally chosen because it was open-source and free to use, but this led to problems during development. The software itself became discontinued toward the end of the project, and the mapping application had to be reprogrammed. Issues like make the user interface vulnerable to changes in the software, which could cause significant problems if it were to be used in the field.

It should be noted that the processing for the radiation data was done after information had been transmitted to the computer. There were several reasons for the decision, including the restrictions to the on-UAV software. The team did not

have open access to the code, and previous researchers had to work with the company to allow the UAV to communicate with the radiation sensor. To make this process as simple as possible, all additional processing was performed after data was transmitted. Additionally, altering the on-UAV software has the potential risk of interfering with the processor's dedicated purpose of flight control, which could lead to additional problems.

5.2 Theoretical Combined System Analysis

Using the chosen commercial UAV and radiation detection sensor, a series of analyses were performed to determine if, theoretically, the combined system would be successful. The characteristics investigated included payload, power draw, flight time, range of travel, and cost.

5.2.1 Payload

The first step in the investigation was to perform a payload analysis. As discussed earlier, payload is one of the most limiting factors when dealing with UAVs. The maximum payload for the X4-C, including its own weight, is 1155 grams. As seen in Table 2 below, the UAV with the various weights of the components is just under its maximum payload. The system was expected to meet requirements, but will have shorter and slower flight times than advertised.

Table 2 – Payload analysis for System A.

System Component	Mass (in g)
Draganfly X4-C	835
Camera Mount	207
GoPro Hero 3+ Camera	73
Geiger Muller Tube	7
Radiation Sensor Circuit	10
Radiation Sensor Attachment	22
Total:	**1154**

5.2.2 Power Draw

An investigation into the power considerations within the system was conducted, since battery life is a major concern when dealing with UAVs. The Draganfly X4-C runs on a 4-Cell Lithium Ion battery that is able to supply 31 watt-hours, allowing the UAV with no attachments to fly for approximately 15 minutes. This time, however, is measured with no payload and without accounting for additional power draw required for data transmission. To determine an accurate time measurement, the power draw analysis in Table 3 was completed. The power draw to operate the data transmission and radiation sensor was determined, as well as the power draw to operate the UAV at full payload capacity. The results show that the additional sensing and transmission elements consist of less than 1% of the system's total power.

Table 3 - Power Draw Analysis for System A.

System Component	Power Draw (in W)
UAV (full payload)	150
Data Transmission	0.1
Radiation Sensor	0.1
Total	**150.2**

5.2.3 Flight Time

Once the power draw analysis was completed, Equation (1) was used to calculate the updated flight time, where T_f is the total flight time in minutes; k_s is the factor of safety; C is the conversion factor from hours to minutes; P_B is the battery power in Watt Hours; and P_{CS} is the total power draw of the combined system. A factor of safety of 0.9 was included to account for any slight variations in power draw due to environmental factors such as wind. Using these parameters, it was determined that the updated flight time was about 12 minutes.

$$T_f = k_s C \frac{P_B}{P_{CS}} \tag{1}$$

The use of the GoPro Hero 3+ as the system's vision component helps to conserve the UAV's battery. This camera is small, inexpensive, lightweight, and with a battery life well over the requirements for the system, approximately 1.5 hours. The live video feed maintains a 12-megapixel resolution, and the 5.8 GHz video receiver allows video to be sent several kilometers.

5.2.4 Range of Travel

Using the information obtained from the flight time analysis, the maximum range of travel for the combined system was determined. As discussed in Section 2, the minimum required area the UAV would need to cover following a dirty bomb

explosion would be about a few city blocks, or about 9 sq. km. The maximum speed of the Draganfly X4-C is 50 km/hour, meaning that it can travel a total of approximately 10 km over the course of its 12-minute battery life. Unfortunately, the data transmission range is far lower than the maximum range of travel. Data transmits at a maximum distance of 2 km in line-of-sight, meaning it is impossible for this design to assess the entire 9 sq. km. Theoretically, this model could be used for small, localized radioactive incidents, but it would not be efficient in dealing with larger-scale radioactive disasters or disaster-sites.

5.2.5 Attachment Analysis

There were several factors to consider when investigating the theoretical feasibility of the designed sensor attachment. It was necessary to consider both the effect the attachment would have on the system, as well as if it could withstand flight. In order to accomplish this task, a simulation of the device in flight was conducted using ANSYS®, a finite element modeling (FEM) software. The simulation was completed in Fluent, ANSYS's fluid analysis tool [21].

In order to complete the ANSYS simulation, the type of flow, whether it was compressible or incompressible, and if it is steady state need to be specified. For the purposes of this analysis, it was assumed that the UAV was traveling at full speed, 50 km/hr., with the nose of the UAV always facing the direction of travel. This assumption was used to simply the problem, so the simulation only needed to be run at one speed and in one direction. Using this assumption, the approximate Reynolds's number (Re) of the flow was calculated using Equation (2). Re is a dimensionless number representing the ratio of the inertial forces to the viscous

forces and is used to determine if a flow can be treated as laminar or turbulent [22]. If the value of Re is less than 10^4, then the flow can be assumed to be laminar. If Re is between 10^4 and 10^6, then the flow is the in transition region between laminar and turbulent. Any value greater than about 10^6 can be assumed to be turbulent [22].

$$Re = \frac{\rho v L}{\mu}$$

The resulting value for Re is 9192, meaning the flow could be treated as laminar. Viscous effects were accounted for by applying boundary layers to the surfaces of the attachment part.

Next, it was determined if the air flow could be treated as incompressible. To do this, the Mach number (M), the ratio of the velocity of the flow to the speed of sound, was calculated. If the value of M is below 0.3, it can be treated as an incompressible flow, meaning it can be assumed that the air within the flow has a constant density [22]. Using equation (3) below, M for this flow was calculated to be 0.041, meaning the incompressible assumption holds.

$$M = \frac{v}{C}$$

(3)

The final assumption made was that the flow was steady state. Using all of these assumptions, a fluid finite element analysis (FEA) was completed to find the approximate drag force acting on the part. After running the simulation, it was determined that the drag was about 0.025 N. This is a negligible about of drag, and

the attachment part is not expected to significantly affect flight. A full description of how this number was obtained can be seen in Appendix A.

Next, to validate the value obtained for the drag force, a rough calculation was done for a simplified version of the part. The attachment piece was approximated as a rectangular prism, which has a drag coefficient of 2.1 [22]. Making this assumption, the approximate drag force was calculated using equation (4) below. This calculated value is expected to be larger than the drag force obtained from the FEA simulation because the approximate cross-sectional area and drag coefficient are larger than the actual part. Using the simplified model, the approximate drag force was calculated to be 0.12 N. This value is in the same order of magnitude as the solution obtained in ANSYS, therefore it is safe to say that the addition of the attachment part will not have a large effect on flight.

$$F_D = \frac{1}{2}\rho A C_D v^2$$

(4)

Using the results from the fluids simulation, the stresses within the part were determined to see if the attachment could theoretically withstand flight. For the top piece of the attachment, PLA has a maximum tensile strength of 66 MPa and the maximum compressive strength 94 MPa [19]. Since the ratio of carbon fiber to nylon is unknown for the bottom piece, an accurate representation of the part's makeup cannot be set in ANSYS. Because of this, the piece was assumed to be entirely nylon, which has a yield strength of 48 MPa [23]. This decision was made because carbon fiber has a considerably higher yield strength than nylon, and if the nylon can withstand flight, the carbon fiber can as well. Using these materials, a

structural analysis was completed and the Von Mises stresses were determined. As seen in Figure 15 below, the largest stress within the part was about 2100 Pa, well below the yield strength for both PLA and nylon, therefore the part will be able to withstand the effects of typical flight.
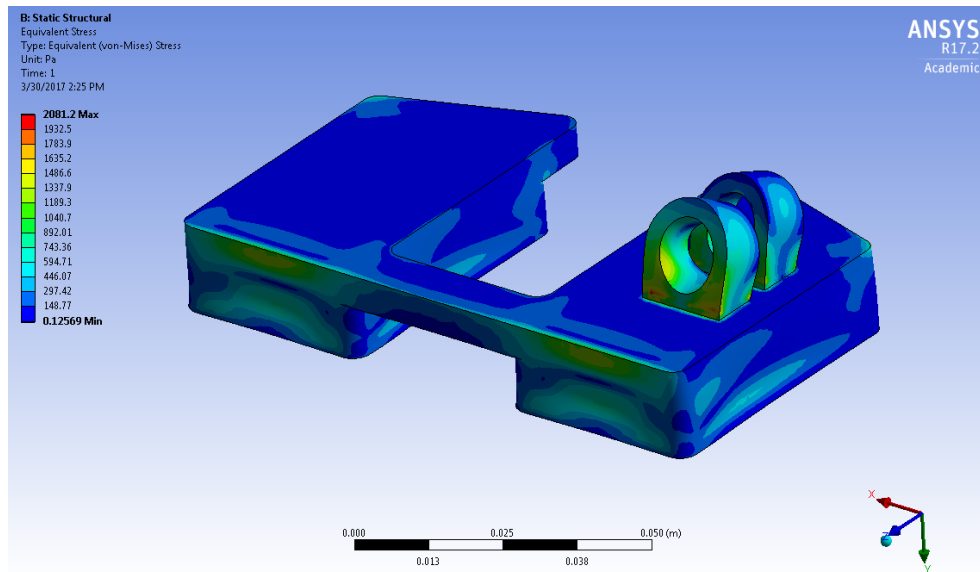
Fig. 15. Von Mises stress distribution within the System A attachment part. The colored bar indicates the stress levels within the attachment, and the black and white bar indicates the size scale. The larger stresses are located where the direction of flow is perpendicular to the attachment part, along the front face. The highest stress is along the front of the Geiger Muller tube attachment, which is due to both the piece's small size and stress concentrations where it connects to the rest of the attachment.

5.2.6 Cost

The final step in the theoretical analysis was to get an approximate cost for the entire system. Looking at the individual system components, the following cost analysis was completed:

Table 4 – Cost Analysis for System A.

System Component	Cost
Draganfly X4-C	$7,000
GoPro Camera	$200
Camera Mount	$2,000
Geiger Muller Tube	$100
Radiation Sensor Components	$25
Sensor Attachment	$5
Total	**$9,330**

After completing this analysis, it was determined that it would cost approximately $9,330 to reproduce this UAV system. This is ignoring factors like labor costs and shipping, meaning that the total cost to a consumer could exceed $10,000.

5.3 Experimental Combined System Analysis

The results of the theoretical analysis performed above in Section 5.2 indicate that the proposed System A meets the requirements of the design task. While it may be quite expensive and have a small flight time, it shows potential to be used in a disaster situation. To further investigate the validity of this design, several experimental analyses were performed to examine the actual flight time and actual data transmission range of the device.

5.3.1 Actual Flight Time

A series of flight tests were conducted to determine the actual flight time of the UAV. The goal of these tests was to determine the amount of time an experienced operator could maintain flight, attempting to keep the UAV in same general 20-meter by 10-meter area, which would represent the high impact zone of a dirty bomb explosion. The UAV was flown in a relatively open area, seen below in Figure 16, with several key obstacles to avoid: a house, a tree line, and several

single trees. These mirror common obstacles the UAV is likely to experience, such as buildings and foliage.

Fig. 16. Testing area for System A flight time experiment (target flight area highlighted).

This testing produced mixed results. Under ideal conditions, low wind, fully charged new battery, the UAV was able to fly for approximately 8 minutes. It could maintain a height several meters above the ground with the full payload. Several images from a successful flight test can be seen below in Figure 17. However, a majority of flight tests produced lower flight times, some as low as one minute. These lower flight times were caused by issues such as environmental factors and battery age.

Fig. 17. System A during flight testing, several meters above the ground.

One of the most limiting factors was the environmental conditions, which greatly affected the operator's control over the UAV. Ideally, this UAV would be used in clear, low wind conditions. Strong wind made the system incredibly difficult to control in flight; even a single strong gust was difficult to recover from during a flight with otherwise minimal wind. This decreased operator control contributed to lower flight times.

Battery age also became an issue; when the battery was new and fully charged, the UAV would fly for longer and at a higher altitude than when fully charged older batteries were used. In some cases, when the older batteries were used, the UAV barely hovered above the ground, as seen below in Figure 18. It is extremely difficult to fly a UAV this close to the ground and increases the risk of a crash. It is impossible to recover the UAV from a crashed position, rendering the UAV useless. Before this UAV design could be implemented, an investigation into the life span of the lithium ion batteries used would be required to determine the time before battery age begins to affect flight performance.

Fig. 18. System A experiencing a hovering issue during a flight test using an older battery.

Another factor limiting the actual flight time of the system is the operator's skill and experience. This specific commercial UAV has a complicated flight control system, and the company recommends attending a weekend long flight training seminar. This training, at a cost of about $2000, adds a significant amount to the estimated cost of the UAV system, increasing the price by about 20%. However, there is a large learning curve when learning to fly the UAV without professional training. Using just written tutorials received from the UAV company, it took the team a substantial amount of time to learn to fly the UAV. Additionally, longer flight times are challenging without considerable practice. This alone would make it difficult to integrate System A into local or state emergency response teams.

5.3.2 Actual Data Transmission Range

In addition to testing the actual flight time, the actual data transmission range of System A was also determined. The data transmission system has a theoretical transmission distance of 2 km. To test this, the UAV was taken to an unpopulated beach, providing an open area with a level ground topography. The UAV remained

at one end of the beach, at a distance of about 3 meters off the ground. The operator with the computer then moved a distance along the beach, recording the time between data transmission points every 50 meters until a maximum distance of 1 km was reached. The test area can be seen below in Figure 19, where the red X indicates where the UAV was placed. The view down the beach from the UAV can be seen in Figure 20.
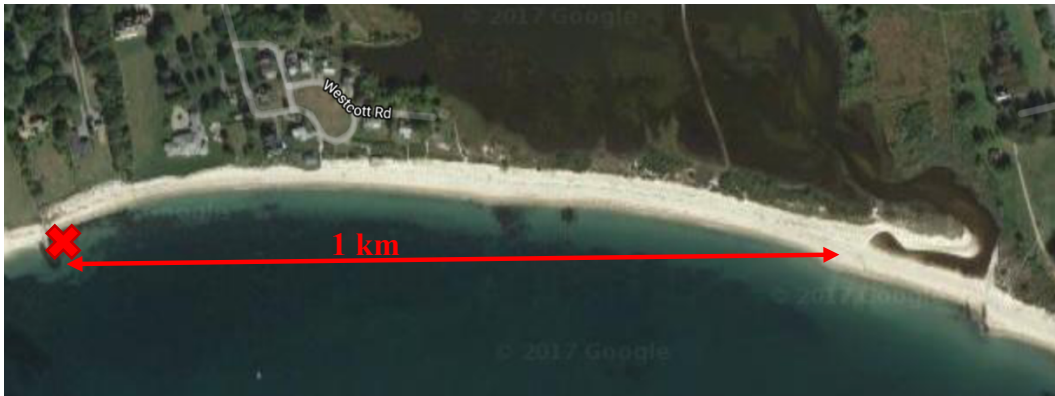

Fig. 19. Aerial view of testing area used for System A data transmission maintaining a line of site experiment.

Fig. 20. Ground view along the beach where the UAV data transmission test was conducted.

The results of testing can be seen below in Table 5, with a visual representation of

in Figure 21. Up to a distance of about 700 meters, the transmission was

continuous, with only the occasional delay in distances between 550-700 meters.

Between 750-850 meters, delays became more common, and beyond about 900

meters delays data transmission was almost impossible. The commercial UAV

used in System A relies on a direct line of sight for data transmission, and many of

these delays were caused by line of sight issues. For example, in distances farther

than about 750 meters, data transmission would completely stop if the receiver,

seen in Figure 22, was not pointed directly at the UAV. Up until about 900 meters,

it was relatively easy to align the two, but beyond this point it was difficult to

establish the correct position for data transmission. It should be noted, however,

that in this test the UAV was not moving. When the device is actually in use, the

UAV will be constantly moving in the air, making it more challenging to align the

two. Because of this, it was determined that the UAV had an experimental data

transmission range of approximately 0.85 km.

Table 5. System A data transmission testing results.

| Distance (m)	Overall Data Transmission	Delays (sec)	Line of Sight Issues
50	Continuous	None	None
100	Continuous	None	None
150	Continuous	None	None
200	Continuous	None	None
250	Continuous	None	None
300	Continuous	None	None
350	Continuous	None	None
400	Continuous	None	None
450	Continuous	None	None
500	Continuous	None	None
550	Mostly Continuous	1-2	Minor
600	Mostly Continuous	1-2	Minor
650	Mostly Continuous	1-2	Minor
700	Mostly Continuous	1-2	Minor
750	Sometimes Continuous	1-3	Medium
800	Sometimes Continuous	1-3	Medium
850	Sometimes Continuous	1-3	Medium
900	Non-Continuous	1-5	Significant
950	Non-Continuous	5+	Significant
1000	Non-Continuous	5+	Significant
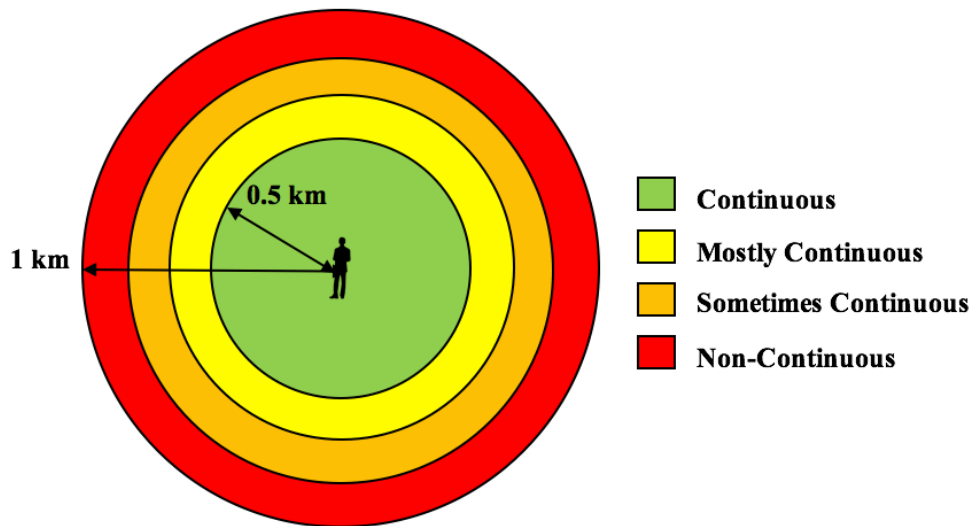
Fig. 21. Visual representation of results obtained from Syste A data transmission testing (shown in Table 5).

Fig. 22. System A receiver. The red arrow indicates the direction that the receiver needs to be pointed directly at the UAV for good line of site transmission.

5.3 Final System Evaluation

Once the theoretical and experimental analyses were completed, the following comparison, as provided in Table 6, was made between the two sets of results. Under ideal conditions, the maximum flight time is not expected to exceed 8 minutes, considerably smaller than the theoretical 12 minutes. Additionally, data transmission range considerably shortens the range of the UAV. Continuous data transmission is only expected to reach a distance of about 0.85 km, which is below size of the theoretical transmission range. This flight distance is significantly smaller than the flight range calculated based on the maximum flight time at maximum speed. Taking all of this information into account, System A is expected to fly for about 8 minutes to a range of about 0.85 km away from the operator.

Table 6. System A theoretical and actual limit comparison.

	Theoretical	Actual
Flight Time	12 minutes	8 minutes
Flight Range (based on flight time at max speed)	10 km	6.7 km
Data Transmission Range	2 km	0.85 km

Since the UAV needs to cover the area surrounding the detonation point, the operator must be within the affected region in order to fully assess the situation. Leaving half a kilometer of distance between the operator and the detonation point, it would take the UAV, at top speed, a little less than a minute to reach the detonation zone. Under ideal conditions, this would only leave about 7 minutes to assess the scene. This further decreases the time the UAV is able to assess the situation, and therefore decreases the efficiency of the model.

The results above show that System A is not capable of efficiently assessing the described disaster situation. It is unlikely that the UAV will be able to fly for the full 8-minute flight time due to issues associated with weather or other environmental conditions. Additionally, the data transmission range is dependent on maintaining a direct line-of-sight between the operator and the UAV. In urban areas, buildings, tress, and other obstructions have the potential to interrupt this connection and prevent the transmission of data. To continue using a model with this much dependence on line-of-sight transmission, development into technologies like swarming UAVs would need to be completed [24]. A swarm of these devices can be used to relay information back to the operator, solving the line of sight issue and extending range. However, this would require extensive research and greatly increase the cost for the overall system.

There are several other issues associated with this design. The commercial UAV used is not designed for autonomous flight, meaning that even with further development, the UAV would still require an operator. As discussed above, this model has a challenging flight control system and weather conditions make it even

more difficult to operate. Because of this, it would be extremely challenging to integrate System A into local and state emergency response teams. Not only is this model no longer in production, it also requires a large amount of training for a single operator, which would increase the cost.

Many of the issues associated with the specific commercial UAV is that it is an outdated model. In the time since the device was purchased, there has been a drastic increase in the number of commercially available UAVs. These newer models are equipped with sophisticated control systems, allowing for easier flight control than the X4-C. Additionally, many of these advanced models are much less expensive than the one used in this prototype. While the estimated cost of System A, about $10,000, is minimal in the event of a serious disaster, a more efficient, cheaper model would be preferable. By marketing this device as a disposable tool for disaster response, it needs to be inexpensive and easily replaceable. Utilizing a newer model could help to accomplish this goal, which lead to the development of System B.

6. Proposed System B

The development of System B consisted of re-evaluating existing UAV technologies and creating a prototype of a new system. While a prototype was created, the corresponding user interface and computer-based data fusion is still under development. A description of this new system is discussed below, as well as a comparison between the two systems.

6.1 Existing Commercial UAV Investigation

After concluding that System A would be inefficient and unlikely to be used for this application, another investigation into existing commercial UAVs was conducted. Newer models from Draganfly Innovations were investigated, along with other UAV companies like 3D Robotics (3DR) and Dà-Jiāng Innovations Science and Technology (DJI). Several different factors were considered during this investigation, including: cost, battery life without a payload, maximum speed, maximum payload, control range, and whether or not autonomous flight was possible. A wide variety of models across different price points were found, and a list of the finding can be seen below in Table 7 [25] [26] [27] [28] [29] [30]. Only models with built-in vision sensing were considered.

Table 7: Existing Commercial UAV Investigation.

Picture	Name	Company	Cost	Battery Life w/out Payload	Max Speed	Max Payload	Control Range	Auto Flight
	AR. DRONE 2.0 GPS EDITION	Parrot	$300	12 min	11.1 m/s	100 g	0.05 km	No
	Solo	3DR	$400	25 min	25 m/s	700 g	0.8 km	Yes
	Phantom 4	DJI	$1,500	28 min	20 m/s	462 g	5 km	Yes
	Inspire 2	DJI	$3,000	27 min	26 m/s	1700 g	7 km	Yes
	Guardian	Draganfly	$7,000	31 min	14 m/s	420 g	0.1 km	No
	X4-P	Draganfly	$13,000	25 min	13.8 m/s	800 g	0.2 km	Yes

After performing this investigation, it was determined that the 3DR Solo would be a good candidate for this application. This specific model has a long flight time, high maximum speed, and autonomous flight capabilities. The Solo is also incredibly affordable; at a price of only $400, it possesses many of the

characteristics of models in much higher price brackets. Additionally, this model is purposely designed to allow developers to make changes and add additional payload systems. All of its software is open-source, and there is a space left on the underside of the UAV for additional payloads to be attached. Because of this, the Solo was chosen as the UAV for System B.

6.2 System Components

System B required a different set of system components than those used in System A and required additional payload development. This model needed additional data transmission hardware and a different software architecture than that used in System A.

6.2.1 Commercial UAV

Like its counterpart used in System A, the 3DR Solo already possessed GPS and live video capabilities, so only the radiation component needed to be added. This system has a flight time of 25 minutes without payload and an advertised 20-minute flight time with maximum payload of 700 grams. The maximum flight speed is about 25 m/s, with a control range of about 0.8 km. The 3DR Solo can be seen below in Figure 23.

Fig. 23. Commercial UAV used for System B, 3DR Solo.

43

This model utilizes a GoPro Hero 4 for live-video, with a streaming video quality of 720p. The camera can either be mounted on a stationary mount or a 3-axis gimbal to allow for operator camera control. These two options allow for system customization. When investigating a small incident in great detail, it would be more beneficial to have increased camera control and the gimbal option can be used. When range is the most important, the lightweight stationary mount can be used to decrease payload weight and increase flight time. These two options can be seen below in Figure 24. When the gimbal is used, however, it blocks two of the attachment screws on the accessory bay, which are required to attach the payload discussed below. Therefore, the stationary mount was chosen for this system.

Fig. 24. Camera mounting options for System B; stationary GoPro mount (left) and 3-axis gimbal mount (right).

6.2.2 Radiation Detection

The radiation sensor developed for System A was recreated for System B, the only slight change being the Geiger Muller tube used. Due to the unavailability of the Canberra Industry tube used in System A, the Sparkfun Geiger Muller tube, COM-08875 ROHS, was used, as seen below in Figure 25. This model has a sensitivity of 1080 CPM in a field of 0.01 mSv as produced by Co60, meaning this tube is a little over twice as sensitive as the one used in System A and therefore meets system

requirements. Fortunately, this model has the same operating voltage as the one used in System A, meaning that the same general circuitry can be used with only slight adjustments; the updated sensor can be seen in Figure 26.
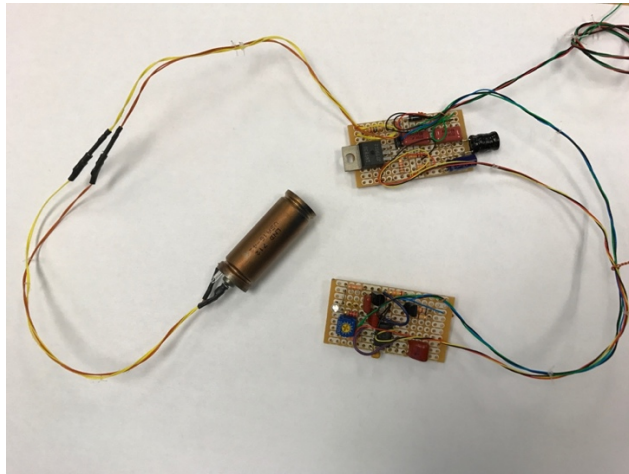

Fig. 25. Geiger Muller tube used for System B.

Fig. 26. Radiation sensor used for System B.
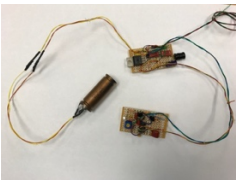
6.2.3 Data Transmission

This UAV has some existing data transmission capabilities. GPS and other telemetry data is transmitted in real time to the operator using the 3DR Link secure WiFi network. However, an issue does arise when transmitting the information from the radiation sensor. The Solo does have the ability to connect additional sensors through a breakout board that can be attached to the bottom side of the UAV. The information, however, can only be saved to the log files, which cannot

be accessed until after flight. Because of this, an additional transmission system is required for the radiation data.

In order to not interfere with the UAV's existing data transmission, which utilizes WiFi, a radio-based transmission was chosen for the radiation data. Once this was determined, a transmission system was designed using commercially available components. This system consisted of two different components: a data transmission system on the UAV and a data receiving system on the the ground. The system components for the initial data transmission system prototype can be seen below in Table 8, while the components for the data receiving system can be seen in Table 9.

Table 8: System B on-UAV data transmission system components.

Picture	Component	Role in System	Notes
	Arduino Uno	Microprocessor	3.3 V reference 500 mA fuse
	Adafruit LoRa Radio Transceiver	Data Transmission	868 or 915 MHz
	LoRa Antenna	Data Transmission	900 MHz
	Battery	Power Supply	9 V
	Radiation Sensor	Radiation Detection	1080 CPM in a field of 0.01 mSv in a field produced by 60Co

Table 9: System B on-ground data receiving system components.

Picture	Component	Role in System	Notes
	Arduino Uno	Microprocessor	3.3 V reference 500 mA fuse
	Adafruit LoRa Radio Transceiver	Data Receiving	868 or 915 MHz
	LoRa Antenna	Data Transmission	900 MHz

The two components use the same general system, the only difference being that the transmission system has a battery and a connection for the radiation sensor. These systems, shown in Figure 27, consist of a transceiver, microprocessor, and an antenna. In transmission system, the radiation sensor sends voltage readings to the microprocessor, which then converts them to CPM and transmits the data to the ground system. The ground system then receives this signal and data is sent to the connected computer. This information can then be combined with the telemetry data, as discussed in the Data Fusion Architecture section below.
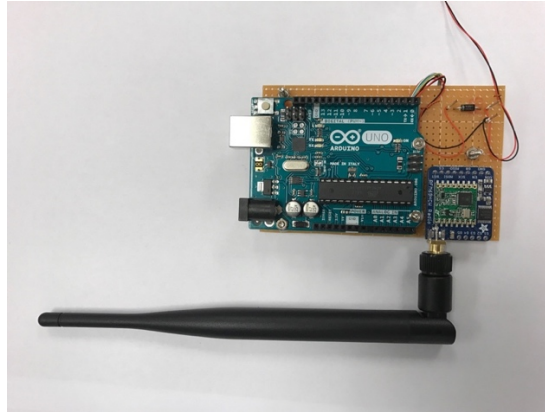
Fig. 27. System B data transmission and receiving system.

It should be noted that the data transmission system discussed above is currently a working prototype, but further development is required for the final system. For example, a smaller processor than the Arduino Uno will be used in the final product. The pieces used were chosen for availability and ease of use for the initial development phase. This initial prototype was used test for any interference issues and if an added payload would affect flight.

6.2.4 Sensing System Attachment

Once the radiation sensor and prototype data transmission circuitry were completed, an attachment was developed to physically integrate the system to the UAV for testing purposes. The process for creating this piece was the same used for System A, were models were produced in SOLIDWORKS and printed in PLA plastic. Due to timing constraints, a carbon fiber and nylon attachment has not yet been produced.

The placement of this component was more straightforward than that of System A. The Solo has a section specifically designed to allow for user created payloads to be attached, as seen in Figure 28. Additionally, no interference issues were found

when the radiation and data transmission system were close to the UAV's existing electronics. Therefore, a design was developed that could be easily installed using the provided 4 screw holes on the Solo.

Fig. 28. 3DR Solo accessory bay on System B.

Because the radiation sensor operates at a high voltage using a kickback generator, it was separated from the other electronics in the data transmission system. To do this, an attachment was created with several different chambers, with slots left open for wires to connect the various systems. The top piece of the attachment, which is directly connected to the UAV, houses the data transmission electronics, as seen in Figure 29. The middle piece then houses the radiation sensor and battery, which each have their own compartment, as seen in Figure 30. This was done to ensure that the pieces would not interfere with each other if they were moved in flight. The bottom piece closes the entire system and holds the Geiger Muller tube, as shown in Figure 31.
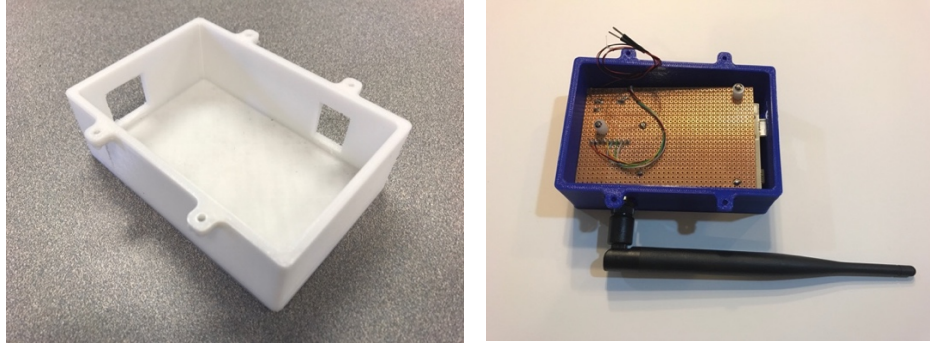
Fig. 29. Top piece of System B payload attachment.
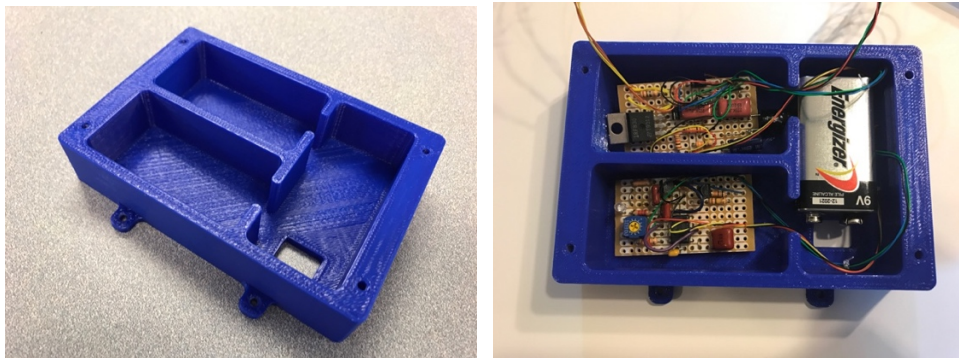

Fig. 30. Middle piece of System B payload attachment.
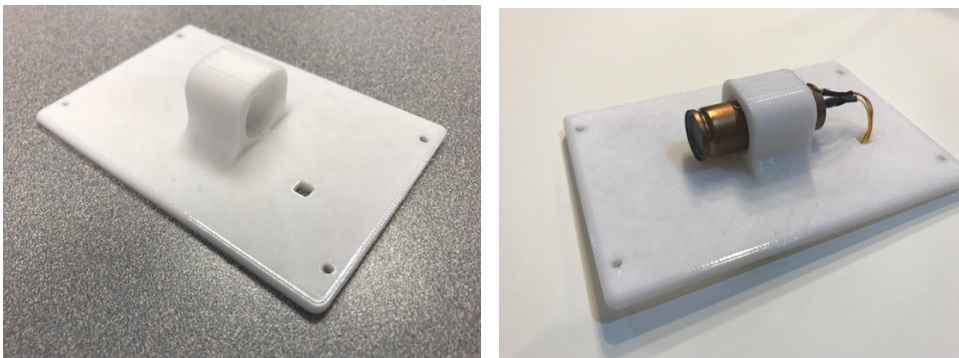
Fig. 31. Bottom piece of System B payload attachment.

Once each of these pieces were produced, the circuitry was installed and the

payload was completed and attached to the UAV, as seen in Figure 32 and 33

respectively.
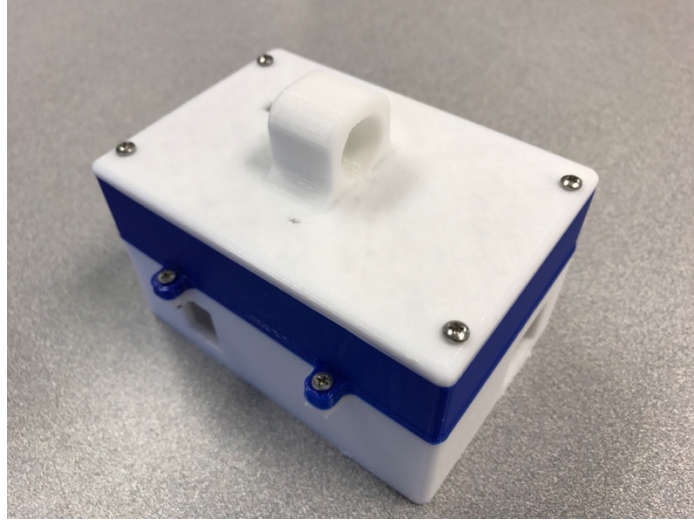
Fig. 32. Completed payload attachment for System B.
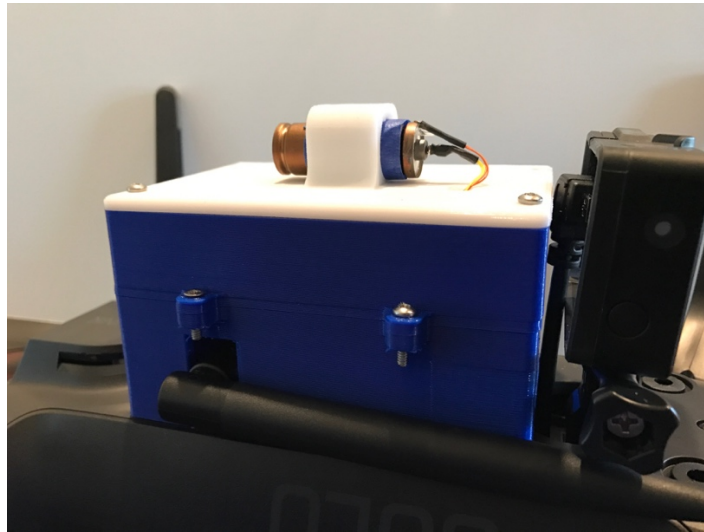
Fig. 33. Installed System B payload attachment.

6.2.5 Data Fusion Architecture

One of the major advantages of using the 3DR Solo is the existing open-source user interface, Mission Planner. Mission Planner is a ground station application that can be used to plan flight paths, monitor the vehicle's in-flight status, and analyze telemetry logs [31]. The user-interface is easy to use, has a GPS map to view the UAV's trajectory, and live-video display capabilities. This means that in order to

create a map of the radiation in the affected area, only the radiation data needs to be added to the existing user interface. An example of the user-interface can be seen below in Figure 34.
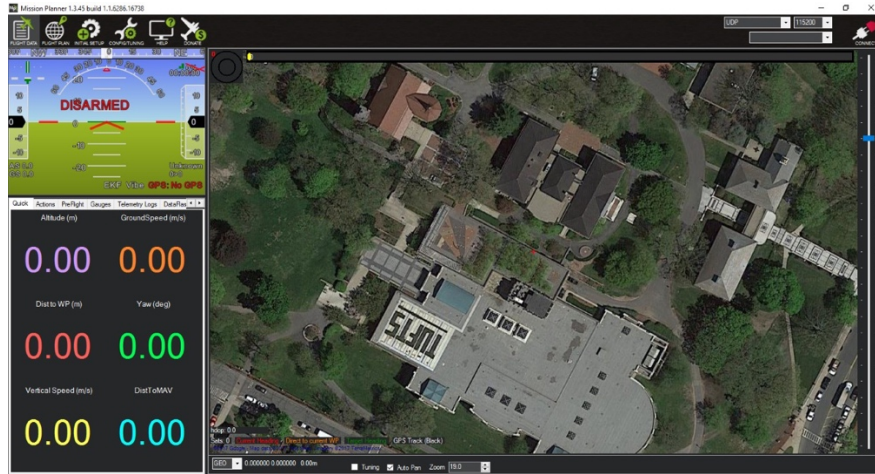
Fig. 34. Mission Planner, System user interface.

Since Mission Planner is completely open source, the data from the radiation sensor transmission system could easily be incorporated. Similar to the interface developed in System A, different colors will be used to represent various radiation levels on the GPS map. This software element, however, is still in development and will be discussed further in the Future Work section.

6.3 Theoretical Combined System Analysis

A similar theoretical analysis used for System A was performed on System B. This would determine if this updated system utilizing a newer commercial UAV would be successful at completing the design tasks. The characteristics investigated included payload, power draw, flight time, range of travel, attachment feasibility, and cost.

6.3.1 Payload

The maximum payload capacity of the 3DR Solo, including its own weight, is 2200 grams. As seen in Table 10 below, the combined weights of the system components is 1802 grams. The value is about 400 grams less than the maximum payload capacity of the UAV, therefore the system is expected to meet flight requirements. It should be noted, however, that since this is just an initial prototype, the later design iterations will likely be lighter due to a smaller data transmission system and smaller payload attachment.

Table 10: Payload Analysis for System B.

System Component	Mass (in g)
3DR Solo	1500
Stationary Camera Mount	50
GoPro Hero 4 Camera	90
Geiger Muller Tube	8
Radiation Sensor	10
Data Transmission System	51
Radiation Sensor/Data Transmission Attachment	93
Total:	**1802**

6.3.2 Power Draw

Unlike System A, the additional sensing components do not run off the UAV's battery power. Because of this, the only factor that needed to be investigated was the power draw when the UAV has the complete attached payload. With full payload, the UAV has an average power draw of about 228 W.

6.3.3 Flight Time

The 3DR Solo advertises a 25-minute flight time with no payload, and it runs off a lithium polymer battery which is able to supply about 76 Watt hours of power. Using the information obtained from the power draw analysis, the theoretical flight time for the combined system was determined using equation (1). The same factor of safety from the System A analysis, 0.9, was used for this calculation. It was determined that the theoretical flight time for System B was about 18 minutes. This number, however, was determined using the maximum payload power draw. Because of this, 18 minutes is the theoretical minimum flight time once the system is completed. The overall payload of the system will be lower than the maximum possible payload, as discussed above in the payload analysis.

6.3.4 Range of Travel

Using the flight time calculated above, the maximum travel distance for the combined system was determined. As discussed earlier, the minimum area following a dirty bomb explosion is approximately 9 sq. km. The maximum flight speed of the 3DR Solo is 90 km/hr, meaning that it can travel about 27 km over the course of its 18-minute battery life. Like System A, however, this range of travel is impacted by the data transmission and control range. For this model, the control range of the UAV is about 0.8 km. While this would give System B a comparable range to System A, a range extender can be added to increase the range to about 4 km. This would allow the UAV the capability to assess the entire 9 sq. km for a dirty bomb explosion. The data transmission system is being developed to have a comparable range to the distance reach with the range extender.

6.3.5 Attachment Analysis

Using the same process used for System A, a finite element analysis was completed for the attachment part developed for System B. Due to the difference in the size of the attachment and speed of the UAV, the assumptions for the analysis needed to be reinvestigated. Using the maximum speed of 89 km/hr., Re was determined to be 163000 using equation (2). This number is about 10^5, meaning the flow is transitioning from laminar to turbulent, and the laminar assumption can no longer be used. Instead, the transition flow settings were utilized in ANSYS. M for the flow was determined to be 0.07 using equation (3), meaning the incompressible assumption still holds. The flow was also assumed to be steady.

Using these assumptions, a similar fluid analysis to the one used for System A was performed. It was determined that the approximate drag force acting on the part was 1.5 N. This value is significantly higher than the value calculated for the attachment in System A. When traveling at top speed, this amount of drag has the potential to effect the system. This attachment, however, is just a prototype to help produce a proof-of-concept for a system utilizing a newer commercial UAV. The final version will be significantly smaller than the current version, which will greatly decrease the overall drag. Additionally, the UAV is not expected to constantly travel at full speed, which will decrease the overall drag[3]. To validate the FEA model, the rectangular prism assumption was used and the approximate drag force was calculated using equation (4). This value was determined to be 2 N,

---

[3] A full description of the FEA analysis used for System B can be found in Appendix B.

which close to the number obtained from ANSYS, showing that the approximation can be used.

Using the results obtained from the fluids simulation, the Von Mises stresses within the attachment were determined. As seen below in Figure 36 and 37, the maximum stress within the part was about 0.06 MPa in the inside of the part, likely due to stress concentrations at the connection points. Since the attachment piece was mad entirely out of PLA, which has a maximum tensile strength of 66 MPa and compressive strength of 94 MPa, it is not expected to yield. This means that the part will be able to withstand a typical flight environment, and the part can be used.
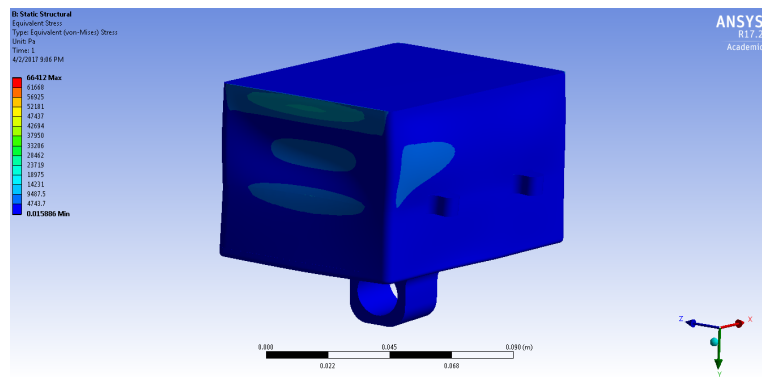

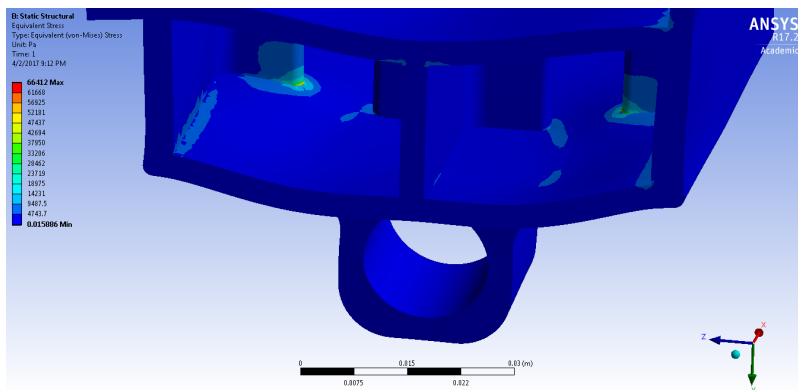Fig. 35. Von Mises stress distribution within the System B attachment part.

Fig. 36. Cross-section view of Von Mises stress distribution within System B attachment part.

57

6.3.6 Cost

One of the biggest advantages to using the 3DR Solo is the drastically lower price compared to the X4-C used in System A. Taking into account the costs of various system components, it was determined that the cost to replicate this prototype UAV system would be about $1,185. Taking into account factors like labor costs and shipping, the estimated total cost of the final product would be around $1,300. This is about 13% of the expected price of System A, meaning it is much more feasible to be integrated into local and state emergency response plans. Additionally, excluding the radiation sensor, every piece used in this design is a commercial off-the-self part, meaning it would be extremely easy to reproduce or fix any damage.

Table 11: Cost Analysis for System B.

System Component	Cost
3DR Solo	$400
GoPro Camera	$200
Camera Mount	$200
Geiger Muller Tube	$94
Radiation Sensor Components	$25
Sensor Attachment	$5
Transceiver (x2)	$60
Arduino Uno (x2)	$24
UAV System Antenna	$12
Ground System Antenna	$5
Range Extender	$160
Total	**$1,185**

6.4 Initial System Testing

Since System B was developed as a proof of concept, and further work is required to produce a finalized system, extensive experimental testing was not completed. For example, the data transmission system produced will not be used in the final

design, but was developed to test radio transmission and its effect on the UAVs own transmission and flight. Because of this, only a series of flight tests were conducted to investigate the flight control of the commercial UAV.

Fig. 37. System B flight test.

The 3DR Solo are simple compared to the X4-C used in System A. After watching a 3-minute instructional video, each of the team members were able to successfully control the UAV. The controls are straight forward and intuitive, and little practice is required to fly a prescribed pattern. In contrast with System A, which took weeks of practice to become a proficient operator, System B has excellent usability. This will make it easier to integrate into emergency response teams, since it will require minimal training. In addition, this UAV also possesses autonomous flight capabilities, where flight paths can be planned and executed through the use of

Mission Planner. This utility has not yet been tested, but initial research and findings indicates that the application should be easy to integrate into flight practices.

6.5 Final System Evaluation

The results of the theoretical analysis and the initial flight tests indicate that this specific design, after completing the remaining development, can be used to efficiently assess a dirty bomb disaster situation. The data transmission system is being specifically designed to have transmission range that matches the control range of the UAV. With this in place, the final system should be able to fly for at least 18 minutes up to a range of about 4 km, all for about $1,300. Under these constraints, the UAV can effectively assess a small, localized radioactive event. Additionally, at such as low price point, the system can be marketed as a disposable tool that is easily replaceable.

It should also be noted that because of the increased range, this UAV allows the first responder to be completely out of the affected region (9 sq. km) and fully assess the area surrounding the detonation point. To be fully out of the affected region, the operator would need to be about 1.7 km away from the detonation point, as seen below in Figure 38. This means at top speed (89 km/hr.), it would take the UAV a little over a minute to reach the detonation point. This leaves 17 minutes to assess the area surrounding the detonation point, a significant increase when compared to the results from System A.
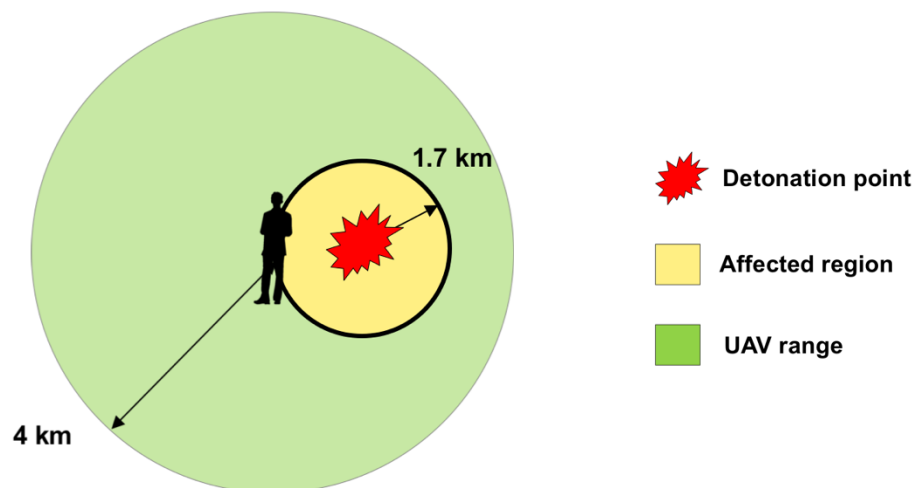
Fig. 38. Range for System B visual.

7. Conclusions and Future Work

Over the course of this research, two commercial UAV systems were developed to assess radiation levels following a dirty bomb explosion. System A was a fully developed system, which combined radiation detection, GPS, and live video to produce a UAV that can be used to assess small radioactive incidents. The results of System A testing showed that in order to produce an effective system, however, newer UAV technologies must be utilized. This led to the development of System B, which showed the true potential of modern commercial UAVs. For a fraction of the price, the 3DR Solo had a flight time over twice as long as the UAV used for System A, all with a larger maximum payload and faster maximum speeds. Additionally, because of available commercial technology like the range extender, the usability range of System B is over 4 times that system A. A full comparison between the two systems can be seen below in Table 12. System B is overall expected to greatly exceed the limits of System A, and once fully developed, it is expected to meet all the design constraints for the project.

Table 12: System A and System B Comparison.

	System A	System B
Flight Time	8 min	18+ min
Range	0.85 km	4 km
Autonomous Flight	No	Yes
Maximum Speed	50 km/hr.	89 km/hr.

As this project is continued, System B will be further developed into a complete prototype. The on-UAV data transmission components are currently being re-evaluated to produce a more compact system, that is expected to be about one forth

of the current size. This will help to decrease the size and weight of the payload, allowing for a smaller payload attachment. In addition to continuing the development of the data transmission, the software component will also be completed. Currently, the radiation data is not integrated into the Mission Planner software. Additional work will be done to integrate the two in order to produce a radiation map similar to the one developed for System A. Once these improvements are made, the System B prototype will be complete and will be tested in a Homeland Security facility.

Overall, the results of this research show that with appropriate sensor integration and data fusion, commercial UAVs can be used as assessment tools in the field of disaster response. This research show that as technology develops, newer, more efficient commercial UAVs will become available, making them better suited for this application. Comparing System A and System B, which were purchased about 4 years apart, highlights this observation. The newer commercial UAV in System B allowed the system to have a longer flight time, faster maximum speed, higher payload capacity, and better flight control, all at a significantly lower price point than A. Additionally, System A does not have the capability for autonomous flight to be developed, while it is an included feature in System B. This allows the system to assess a larger area more efficiently, all without significant operator training. In less than 5 years, the technology available drastically improved in the commercial UAV market, and this improvement is expected to continue in the next few years. Taking this into account, the same methodology used to develop the prototypes discussed in this research can be used by future developers to produce affordable,

effective tools for all areas of disaster response. This research focused on applications for radioactive disasters, but this could be expanded to countless other disaster situations.

8. Appendices

Appendix A: FEA for System A

Using the assumptions discussed in section 5.2.5, a fluid and structural simulation and analysis was completed for System A. Since this analysis was just a rough approximation to ensure that the payload attachment would be able to withstand flight, several assumptions were made to the model. In order to have a correct fluid analysis, both the attachment piece and all other UAV components need to be represented. To simplify this, all other UAV components were modified to just be simple shapes, since in Figure 39 below. The large upper box is used to represent the UAV's main cavity, and the lower boxes represent the other components of the camera mount. These components have the approximate dimensions as their corresponding actual parts. The legs and propellers of the UAV were neglected.
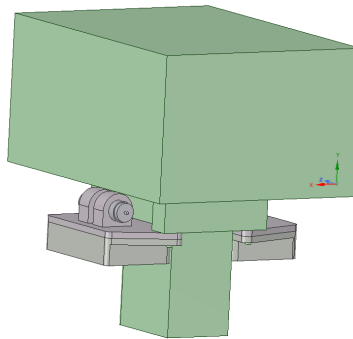

Fig. 39. Simplified model used for System A FEA analysis.

Once the physical components were completed, the fluid medium was created. To do this, a fluid enclosure was created surround the solids, which were then suppressed from the model. The results of this fluid space an be seen below in Figure 40.
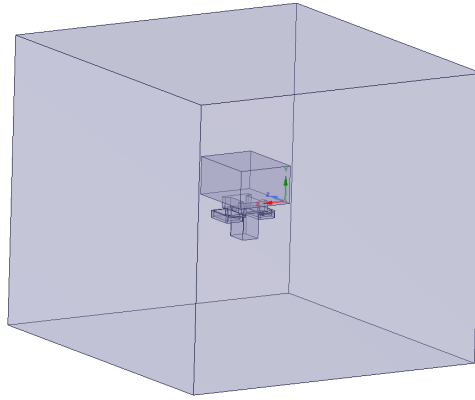
Fig. 40. Fluid enclosure used for System A fluid FEA analysis.

Once the fluid model was created, the mesh was completed. Because viscous effects need to be accounted for, a boundary layer need to be applied to the surfaces of the fluid around the solid part. This includes not only the sensor attachment, but the approximations of the surrounding system components as well. A zoomed in view of a boundary layer can be seen below in Figure 41.
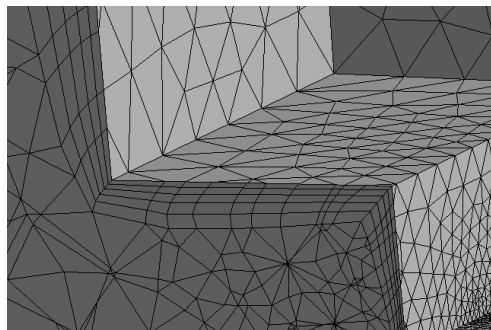

Fig. 41. Boundary layers created for FEA analysis

Once all the boundary layers were applied, the rest of the mesh was completed. Using proximity with curvature, a fine mesh was generated; a cross-sectional view of the mesh can be seen in Figure 42 below. In order to determine the mesh quality, the skewness and orthogonal quality were determined. When creating an ANSYS simulation, the ideal skewness is 0, and the ideal orthogonal quality is 1. For this

analysis, the skewness was about 0.2 and the orthogonal quality was about 0.9. For the purposes of this simplified analysis, these values indicate that the mesh can be used.
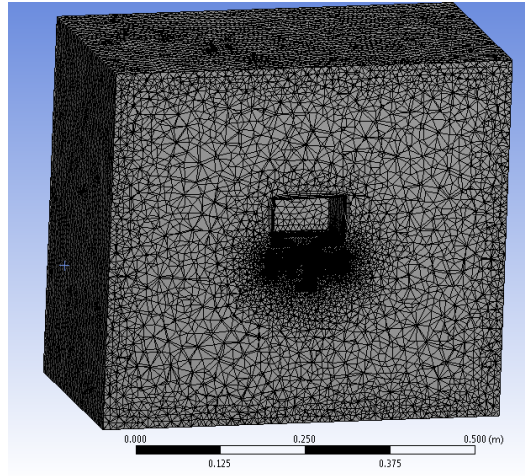

Fig. 42. Completed mesh for System A, cross-sectional view

Once meshing was completed, boundary conditions were applied to the model. The inlet was defined to have a speed of 13.89 m/s, the maximum speed of the UAV. The outlet was defined as a pressure driven outlet, and the remaining fluid surfaces were classified as symmetry. Finally, the attachment and other UAV components were defined as wells. Using these boundary conditions, the simulation was then completed. The drag acting on the just the attachment plot was monitored, and enough iterations were completed such that the drag approached a constant value, 0.025 N.

Once the drag was determined, the information from the fluid simulation was transferred to an ANSYS static structural analysis. In this new structural simulation, only the attachment part was investigated. The pressure acting on the part from the fluid analysis was imported into the model and applied to the exposed

surfaces of the part. Then a fixed support was applied to the surface of the attachment piece connected to the camera mount.

Once the forces and boundary conditions were applied, the structural analysis was completed. The Von Mises stress plot shown in 5.2.5 was produced, along with the strain and displacement plots shown below in Figures 43 and 44. As discussed above, the results of this FEA analysis show that the attachment piece is expected to withstand flight and meets the qualifications of the design.
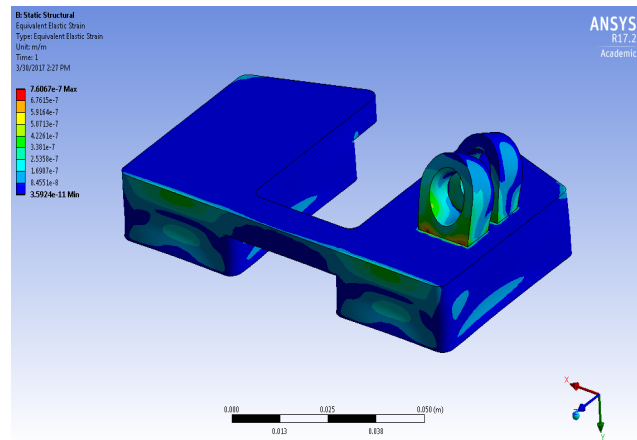

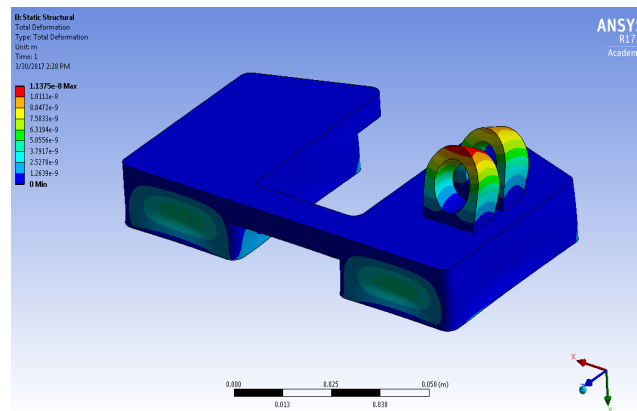Fig. 43. Von Mises strain distribution in System A attachment part

Fig. 44. Displacement in System A attachment part

Appendix B: FEA for System B

As discussed in section 6.3.5, the FEA simulation for System B required transitional flow instead of laminar; other than this change, the same general analysis completed for System A was completed for System B. The approximate parts for the UAV were created, and the solid and fluid models can be seen below in Figures 45 and 46 respectively. A mesh was then generated in the same manor used for System A, with boundary layers applied to each solid surface. The finished mesh can be seen in Figure 47. This mesh had a skewness of 0.21 and an orthogonal quality of 0.87, meaning the mesh will be sufficient for the analysis.
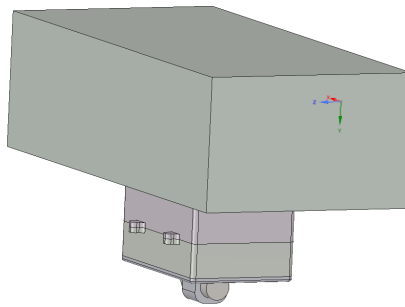

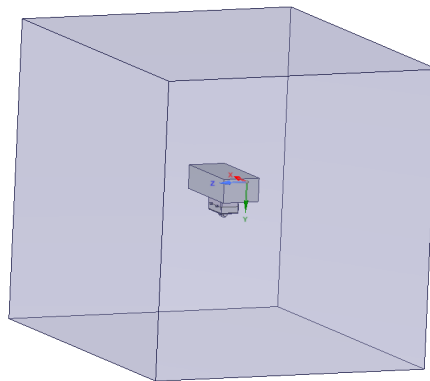Fig. 45. Simplified model used for System B FEA analysis.

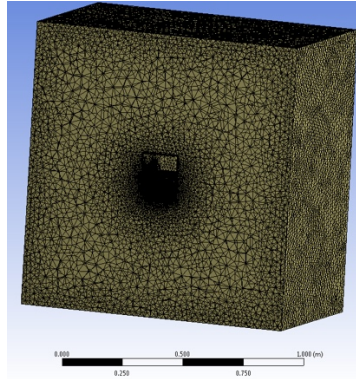Fig. 46. Fluid enclosure used for System B fluid FEA analysis.

Fig. 47. Completed mesh for System B, cross-sectional view

Once the mesh was completed, boundary conditions were applied. The inlet was defined to be the maximum speed of the UAV, 24.7 m/s. Like the System A analysis, the outlet was defined as a pressure driven outlet, and the remaining fluid surfaces were classified as symmetry. The attachment and other UAV components were then defined as wells. A transitional flow simulation was then completed. The drag acting on the attachment plot was monitored, and enough iterations were completed such that the drag approached a constant value, 2 N.

Once the fluid analysis was completed, the pressure acting on the part was transferred to a static structural analysis. A fixed support was applied to the top surface of the part, where it is attached to the UAV. Then the structural analysis was completed, and the stress, strain, and displacement in the part were plotted. The Von Mises stress distribution can be seen above in section 6.3.5, and the strain and displacement can be seen below in Figures 48 and 49 respectively. As already discussed, the results of this FEA analysis show that the attachment part is expected to withstand flight and will meet system requirements.
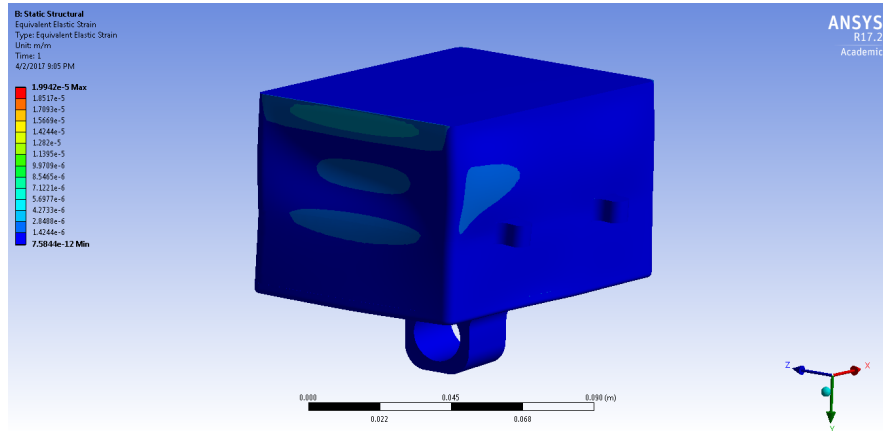
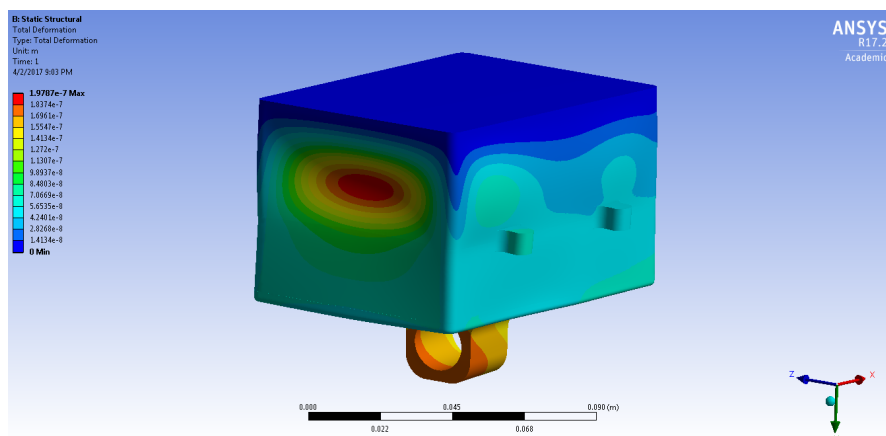Fig. 48. Von Mises strain distribution in System B attachment part

Fig. 49. Displacement in System B attachment part

Appendix C: Schematic for System A radiation sensor

Fig. 50. Schematic for System A radiation sensor

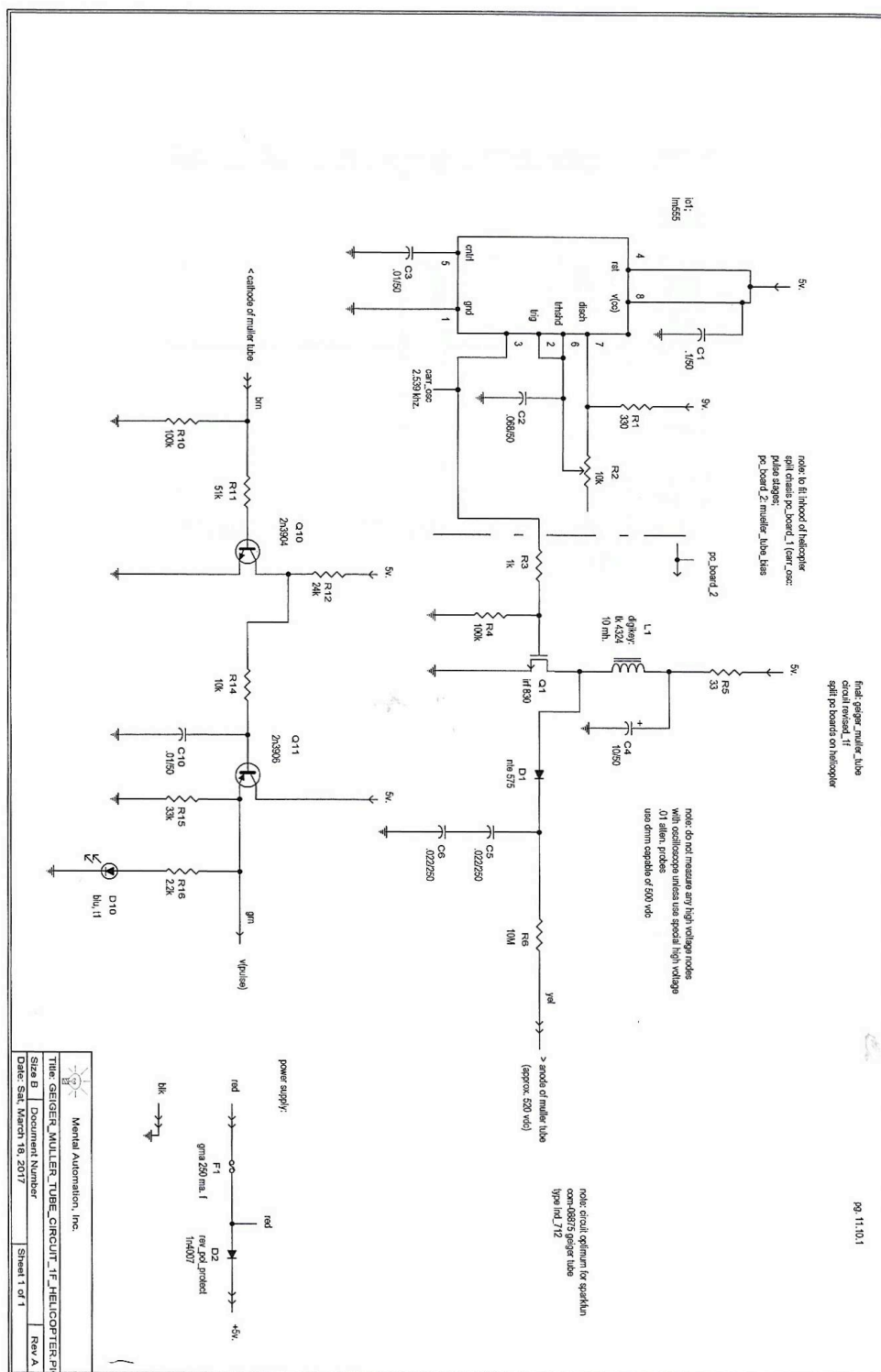# Appendix D: Schematic for System B radiation sensor

Fig. 51. Schematic for System B radiation sensor

9. References

[1]   K. L. B. Cook, "The Silent Force Multiplier: The History and Role of UAVs in Warfare," *2007 IEEE Aerospace Conference*, Big Sky, MT, 2007, pp. 1-7.

[2]   Hayden, M. V. "To Keep America Safe, Embrace Drone Warfare." *New York Times* 19 Feb. 2016: n. pag. Print.

[3]   "Aerial Photography with Drones." *Unmanned Applied Solutions*. N.p., n.d. Web. 11 Mar. 2017.

[4]   A. Ali, N. Ballou, B. McDougall and J. L. Valle Ramos, "Decision-support tool for designing small package delivery aerial vehicles (DST-SPDAV)," *2015 Systems and Information Engineering Design Symposium*, Charlottesville, VA, 2015, pp. 45-50.

[5]   Baxter, R. A., and D. H. Bush. "Use of Small Unmanned Aerial Vehicles for Air Quality and Meteorological Measurements." National Ambient Air Monitoring Conference. Atlanta. 2014. Web. 11 Feb. 2017.

[6]   P. Rudol and P. Doherty, "Human Body Detection and Geolocalization for UAV Search and Rescue Missions Using Color and Thermal Imagery," *2008 IEEE Aerospace Conference*, Big Sky, MT, 2008, pp. 1-8.

[7]   Murphy, Douglas W., and James Cycon. *SAO/NASA ADS: ADS Home Page*. Proc. of Applications for Mini VTOL UAV for Law Enforcement, Boston. Sensors, C3I, Information, and Training Technologies for Law Enforcement, 01 Jan. 1999. Web. 30 Mar. 2017.

[8]   Smith, Matt. "Flying Drone Peers into Japan's Damaged Reactors." *CNN*. Cable News Network, 10 Apr. 2011. Web. 30 Jan. 2017.

[9]   T. Giitsidis, E. G. Karakasis, A. Gasteratos and G. C. Sirakoulis, "Human and Fire Detection from High Altitude UAV Images," *2015 23rd Euromicro International Conference on Parallel, Distributed, and Network-Based Processing*, Turku, 2015, pp. 309-315.

[10]   N. Davis, F. Pittaluga and K. Panetta, "Facial recognition using human visual system algorithms for robotic and UAV platforms," *2013 IEEE Conference on Technologies for Practical Robot Applications (TePRA)*, Woburn, MA, 2013, pp. 1-5.

[11]   "Fact Sheet on Dirty Bombs." *United States Nuclear Regulatory Commission*. N.p., n.d. Web. 11 Mar. 2017.

[12]   "RADIOLOGICAL ATTACK DIRTY BOMBS AND OTHER DEVICES." Department of Homeland Security, 2004. Web. 11 Mar. 2017.

[13]   Lee, B. "How Much Radiation Is Too Much?" *PBS*. Public Broadcasting Service, 22 Mar. 2011. Web. 11 Mar. 2017.

[14]   "Radiation and Life." *World Nuclear Association*. N.p., Dec. 2012. Web. 11 Mar. 2017.

[15]   Knoll, Glenn F. *Radiation Detection and Measurement*. New York: John Wiley & Sons, 1979. Print.

[16] " *Geiger-Muller Tube*. Digital image. *Wikipedia*. N.p., 2017. Web. 10 Apr. 2017.

[17] Schweig, Andrew. *Automated Threat Detection for Disaster Response Teams Using UAV Platforms*. Thesis. Tufts University, 2013. N.p.: n.p., n.d. Print.

[18] "Radiation Basics." *United States Nuclear Regulatory Commission*. N.p., 17 Oct. 2014. Web. 11 Mar. 2017.

[19] "PLA and ABS Strength Data." *MarkerBot*. N.p., n.d. Web. 29 Mar. 2017.

[20] " Scott, Chris. "Nylon." *Polymer Processing*. N.p., n.d. Web. 30 Mar. 2017.

[21] "Simulation Driven Product Development." *ANSYS*. N.p., n.d. Web. 29 Mar. 2017.

[22] White, Frank M. *Fluid Mechanics*. Vol. 7. New York: McGraw-Hill, 2011. Print.

[23] McCue, TJ. "Is Your 3D Printing Material Tough Enough?" *Lifewire*. N.p., 17 Oct. 2016. Web. 29 Mar. 2017.

[24] Allison, Robert, Charles V. Peña, Harry J. Kazianis, and W. James Antle III. "Can Drone Swarms Save America's Aircraft Carriers?" *The National Interest*. The Center for the National Interest, 17 Oct. 2016. Web. 29 Mar. 2017.

[25] "Solo Specs." *3DR*. N.p., 2016. Web. 10 Feb. 2017.

[26] "Phantom 4." *DJI Official*. N.p., 2017. Web. 11 Feb. 2017.

[27] "Inspire 2." *DJI Official*. N.p., 2017. Web. 11 Feb. 2017.

[28] "Draganfly Guardian." *Draganfly Innovations Inc.* N.p., 2016. Web. 11 Feb. 2017.

[29] "Draganfly X4-P." *Draganfly Innovations Inc.* N.p., 2016. Web. 11 Feb. 2017.

[30] "Parrot AR. Drone 2.0 GPS Edition." *Parrot*. N.p., 2016. Web. 11 Feb. 2017.

[31] "Mission Planner Overview." *Ardupilot*. N.p., 2016. Web. 29 Mar. 2017.

[32] K. L. B. Cook, "The Silent Force Multiplier: The History and Role of UAVs in Warfare," *2007 IEEE Aerospace Conference*, Big Sky, MT, 2007, pp. 1-7.